426
Copy
RM H58C14

NACA RM H58C14

Declassified by authority of NASA Classification Change Notices No. 209
Dated **11-30-70

RESEARCH MEMORANDUM

CLASSIFICATION CHANGED
UNCLASSIFIED
To
By Authority of NASA TO 70-59 Date 10/19/70

INDUCTION SYSTEM CHARACTERISTICS AND ENGINE SURGE OCCURRENCE FOR TWO FIGHTER-TYPE AIRPLANES

By Terry J. Larson, George M. Thomas,
and Donald R. Bellman

High-Speed Flight Station
Edwards, Calif.

FACILITY FORM 602
N71-70251 (ACCESSION NUMBER)
(THRU)
37 (PAGES)
none (CODE)
(NASA CR OR TMX OR AD NUMBER)
(CATEGORY)

NATIONAL ADVISORY COMMITTEE
FOR AERONAUTICS

WASHINGTON
May 26, 1958

CONFIDENTIAL

NATIONAL ADVISORY COMMITTEE FOR AERONAUTICS

RESEARCH MEMORANDUM

INDUCTION SYSTEM CHARACTERISTICS AND ENGINE SURGE OCCURRENCE FOR TWO FIGHTER-TYPE AIRPLANES

By Terry J. Larson, George M. Thomas,
and Donald R. Bellman

SUMMARY

An investigation was conducted to measure and to compare the total-pressure recovery and distortion characteristics at the compressor face of two single-place fighter-type airplanes with similar two-spool turbojet engines, but with dissimilar inlets. Airplane A has a single normal-shock nose inlet; airplane B has two engines and triangular-shaped inlets located in the wing roots. In addition, data are presented for engine surge occurence of these two airplanes and also for a third single-engine airplane having two semicircular-shaped side inlets.

The total-pressure recovery was relatively independent of angle of attack and mass-flow ratio for both airplanes except for a significant decrease in pressure recovery with angle of attack for airplane B at the highest Mach numbers tested. The root-mean-square total-pressure distortion decreased slightly with angle of attack and increased slightly with mass-flow ratio for airplane A. For airplane B the distortion increased with angle of attack and decreased slightly with mass-flow ratio, particularly at the higher altitudes. Altitude effects on distortion were noted only for airplane B.

Engine compressor surges were encountered primarily in the region of high altitude and low inlet total pressure, as indicated by wind-tunnel tests. At lower altitudes and at higher inlet total pressure, surges were encountered under conditions of high total-pressure distortion, particularly circumferential distortion.

INTRODUCTION

Air-flow characteristics of air inlets and ducts of jet airplanes have a significant effect on the performance of the airplanes. Of these

CONFIDENTIAL

characteristics pressure recovery is important, but flow distortion is sometimes more important. A large degree of flow distortion can limit engine performance by causing surging in the engine compressor; that is, a stalling of all compressor stages with a rapid fluctuation of air flow.

The air-flow characteristics of a given inlet can vary with altitude, Mach number, inlet-flow angles, engine speed, and other parameters. Since it is difficult to exactly simulate flight conditions in a wind tunnel, a flight investigation was made at the NACA High-Speed Flight Station at Edwards, Calif., to measure inlet-flow distortion and total-pressure recovery at the compressor face on three fighter- or interceptor-type airplanes with similar turbojet engines. A part of this investigation was devoted to the determination of surge characteristics of these airplanes. Since compressor surges can be damaging to the airplane, the number of surges encountered was necessarily limited. However, enough data were obtained to present a brief comparison of the surge characteristics of the three airplanes. Because the data from the third airplane have been reported previously in reference 1, only the surge data for this airplane are included in the present paper for comparison.

The pressure-recovery data were obtained primarily over a Mach number range from 0.8 to 1.4 and at altitudes between 22,000 feet and 42,000 feet. Compressor surges were encountered at Mach numbers from 0.6 to 1.5 and at altitudes between 30,000 feet and 52,000 feet.

SYMBOLS

A	cross-sectional area, sq ft
D	circumferential distortion factor, $\left(\frac{p'_{max} - p'_{min}}{p'_{av}}\right)\left(\frac{\theta-}{180}\right)\left(\frac{\theta+}{180}\right)100$, percent
h_p	pressure altitude, ft
M	Mach number
m/m_0	mass-flow ratio, $\frac{\text{Duct mass flow}}{\rho_0 V_0 A_i}$
N	engine inner-rotor speed, rpm
$N/\sqrt{\theta_c}$	normalized engine inner-rotor speed, rpm

n	number of total-pressure probes
p	static pressure, lb/sq ft
p'	total pressure, lb/sq ft
p'_{av}	average total pressure of the five total-pressure rakes, lb/sq ft
p'_{max}	highest of the averaged pressures of the five total-pressure rakes, lb/sq ft
p'_{min}	lowest of the averaged pressures of the five total-pressure rakes, lb/sq ft
R	Reynolds number based on minimum area equivalent circle diameter
S	root-mean-square distortion, $\left(\sqrt{\frac{\sum \varphi^2}{n-1}}\right)100$, percent
T'	inlet air total temperature, $^{\circ}R$
V	velocity, ft/sec
w_a	air-flow rate, lb/sec
$\frac{w_a\sqrt{\theta_c}}{\delta_c}$	normalized air flow, lb/sec
x	distance from inlet, in.
α	angle of attack, deg
δ_c	pressure normalizing factor, $\frac{p'_c}{\text{Sea-level static pressure}}$
θ	compressor-face circumferential station, deg
θ_c	temperature normalizing factor, $\frac{T'_c}{\text{Sea-level static temperature}}$

$\theta-$ circumferential angle subtended by the largest singly connected sector of the inlet annulus, having a total pressure less than the average (see diagram)

$\theta+$ circumferential angle subtended by the largest singly connected sector of the inlet annulus, having a total pressure greater than the average (see diagram)

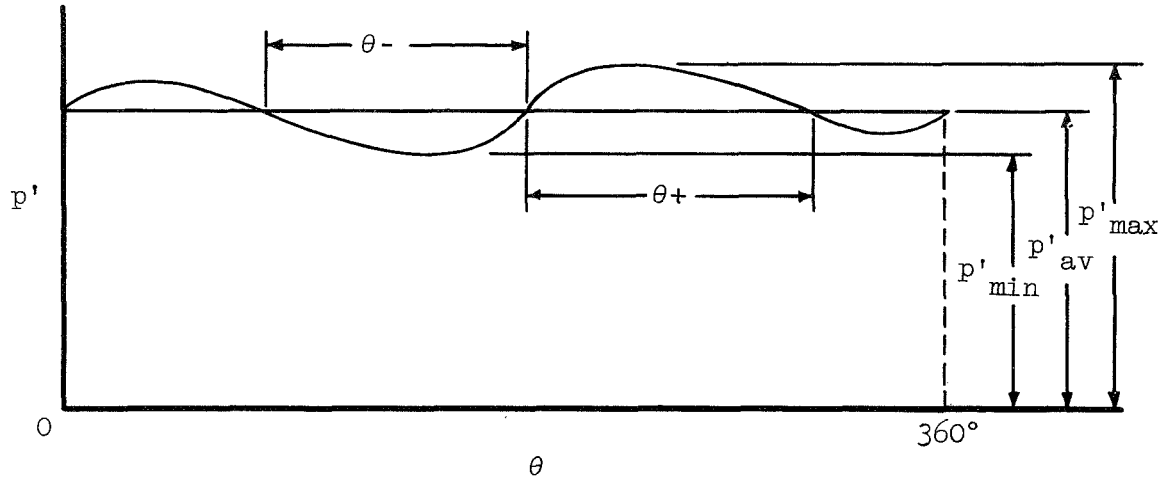

ρ air density, slugs/cu ft

φ compressor-face total-pressure distortion factor, $\left[\left(\frac{p'_l}{p'_0}\right) - \left(\frac{p'_l}{p'_0}\right)_{av}\right]$

Subscripts:

0 free stream

av average

c compressor face

i inlet

l local

AIRPLANES

The three airplanes are single-place fighter- or interceptor-type airplanes powered by similar two-spool turbojet engines with afterburners. The following are details of the airplanes and their inlet and duct systems.

Airplane A

The engine of airplane A is supplied air through a single normal-shock-type nose inlet. Figures 1 and 2 are photographs of the airplane and the nose inlet, respectively, and figure 3 is a drawing showing the duct contours and area distribution. The inlet has a lip radius of about 0.25 inch, and the diffuser has an equivalent conical expansion angle (included wall angle of a frustrum of a cone having the same length and inlet and exit areas) of 0.37°. Detailed dimensions and other physical characteristics of the airplane are presented in reference 2.

Airplane B

Airplane B is powered by two engines to which air is supplied by triangular-shaped inlets located in the wing roots. Each inlet supplies air to one engine. Figures 4 and 5 are photographs of the airplane and the inlet, respectively, and figure 6 is a drawing showing the duct contours and area distribution. The inlets have elliptical lips with a minimum radius of about 0.3 inch, and the diffusers have an equivalent conical expansion angle of 1.72°. Detailed dimensions and other physical characteristics of the airplane are presented in reference 3.

Airplane C

Air is supplied to the engine of airplane C by two semicircular-shaped side inlets which converge ahead of the compressor face. Figures 7 and 8 are photographs of the airplane and the inlet, respectively, and the duct contours and area distribution are shown in figure 9. Each inlet has a lip radius of 0.25 inch, and the diffuser has an equivalent conical expansion angle of 1.07°. Additional details on the airplane, duct, and duct instrumentation are given in reference 1.

INSTRUMENTATION AND ACCURACY

Each airplane duct was instrumented primarily at the compressor face where five radial rakes for measuring total pressures were installed. Figure 10 shows the circumferential locations of these rakes as well as the radial positions of the probes for airplanes A and B.

The compressor-face probe pressures were measured by NACA mechanical-optical manometers which determine the difference between the probe and the reference pressures within ±5 pounds per square foot. The flow-distortion values are based on differential pressures and, hence, were accurate to ±5 pounds per square foot. The total-pressure recovery at the compressor face required the measurement of a reference pressure. For airplane A this measurement was made with an absolute manometer cell having an accuracy of ±20 pounds per square foot; for the other two airplanes the reference pressure was determined by a more sensitive method, allowing an accuracy of ±5 pounds per square foot.

For all three airplanes Mach number accuracy is believed to be within ±0.01 at subsonic and supersonic speeds and within ±0.02 at transonic speeds. Angle of attack was measured to an accuracy of about 0.5°.

RESULTS AND DISCUSSION

The pressure-recovery data were obtained primarily over a Mach number range from 0.8 to 1.4 and at altitudes between 22,000 feet and 42,000 feet. Compressor-surge data were obtained at Mach numbers from 0.6 to 1.5 and at altitudes between 30,000 feet and 52,000 feet. These data correspond to a Reynolds number range from 1.4×10^6 to 9.2×10^6, based on minimum-area equivalent circle diameter.

Compressor-Face Total-Pressure Surveys

Contours for every 5 percent of the total-pressure recovery are shown for the compressor face for airplane A in figure 11 for a range of angle of attack at Mach numbers of about 0.80, 1.0, and 1.4. A comparsion of the contour plots shows that the distortion is small and, evidently, is not affected by either angle of attack or Mach number for the ranges presented. The total-pressure recoveries are relatively high, with the lowest recoveries occurring at the bottom of the duct for Mach numbers of 0.8 and 1.0.

Figure 12 presents the same data as shown in figure 11 in a different, more objective manner. The average total-pressure recovery of all

probes on each rake is shown as a circle with a solid line connecting these values. The radial location of each probe and the circumferential location of each rake are both indicated on the abscissa. The dashed line indicates the average total-pressure recovery of all the rakes. From figure 12 it can be seen that angle of attack slightly affects circumferential distortion, especially near the 180° region where the total-pressure recovery begins dropping when angle of attack increases beyond 8°.

Figure 13 shows the variation of total-pressure recoveries and total-pressure distortions with mass-flow ratio and angle of attack at the compressor face of airplane A. For the lower Mach number range and for mass-flow ratios between 0.90 and 1.00 total-pressure recovery decreases about 2 percent as the angle of attack increases from about 0.5° to over 19°. Fairings are not shown for some of the sets of points because of the large scatter. This scatter is most likely a result of the reference cell, noted in "Instrumentation and Accuracy," on which the computations of pressure recovery and mass-flow ratio depend. Despite the scatter, the data indicate that the pressure recovery is high throughout the mass-flow range tested and varies little with mass-flow ratio, indicating that for these tests no choking occurred.

The root-mean-square distortion of the total pressure plotted against angle of attack (fig. 13) shows the distortion dropping from about 3 percent at an angle of attack near 0.5° to slightly less than 2 percent at an angle of attack somewhat greater than 19°. The distortion also varies slightly with mass-flow ratio, changing from about 1.5 percent to about 3.0 percent as the mass-flow ratio increases from 0.65 to 0.99.

Figures 14 and 15 present total-pressure-recovery plots for airplane B comparable to those in figures 11 and 12 for airplane A. Figure 14 shows that angle of attack affects both circumferential and radial distortion at the compressor face. It is evident from figure 15 that, similar to airplane A, the lowest total-pressure recoveries are experienced near the bottom of the duct. The average total-pressure recoveries at a Mach number near 1.0 vary from 0.953 to 0.930 in figure 15(b), corresponding to an angle-of-attack change from 3.3° to 10.7°. Figure 15(c) shows a similar variation for Mach numbers near 1.4.

Presented in figure 16 are the variations of average total-pressure recovery and total-pressure distortions with angle of attack and mass-flow ratio at the compressor face of airplane B. For the curve showing total-pressure recovery plotted against angle of attack the transonic data are for mass-flow ratios between 0.9 and 1.0, whereas the supersonic data are for mass-flow ratios between 0.85 and 0.95. In the transonic range the total-pressure recovery drops from approximately 0.95 to 0.94

[redacted]

when the angle of attack is increased from 0° to about 11°. The supersonic total-pressure recovery appears to be more sensitive to angle of attack. At an angle of attack near 0° the recovery is 0.925, while at an angle of attack of 8° it is approximately 0.86. Very little variation in total-pressure recovery is evidenced as the mass-flow ratio increases from about 0.88 to about 1.00, indicating unchoked flow in the duct.

Figure 16 shows that the root-mean-square total-pressure distortion increases with altitude as well as with angle of attack. At an angle of attack of 8° and at a pressure altitude of 50,000 feet the distortion is 6.4 percent, at 40,000 feet it is 5.2 percent, and at 30,000 feet (by extrapolating) it is near 4.4 percent. The root-mean-square distortions of the total pressures for three pressure altitudes plotted against mass-flow ratio indicate little variation in distortion as the mass-flow ratio increased from 0.88 to 1.00.

Surges Encountered

Several compressor surges were encountered for each airplane. Table I lists flight and compressor-face conditions that occurred immediately prior to the surges. In order to summarize the surge regions and to help analyze the surges, figure 17 presents pressure altitude plotted against Mach number immediately prior to surge. NACA Lewis altitude wind-tunnel tests of a similar engine show that compressor surge can occur at low Reynolds numbers corresponding to total pressures less than about 500 pounds per square foot for normal bleed-door operation and no distortion. These conditions are shown by the shaded region in figure 17.

Reference 1 shows that for airplane C the compressor-face distortions for surge data are not significantly different in magnitude from the distortions for nonsurge data and therefore concludes that distortion was not responsible for the surges experienced by this airplane. Reference 1 showed, too, in a manner similar to that used in figure 17, that good agreement is obtained between wind-tunnel data and full-scale flight data in establishing the surge region of this particular engine.

As can be seen in figure 17, two of the three compressor-surge points for airplane A also occur at total pressures less than 500 pounds per square foot. However, the surge point shown at a Mach number of 0.756 was accompanied by a root-mean-square distortion at the compressor face which is considerably greater than normal for this airplane (fig. 13 and table I). Although the total pressure at the compressor face exceeds 500 pounds per square foot only by 40 pounds per square foot, it is believed that the surge was caused by the relatively high distortion;

[redacted]

this distortion was undoubtedly a result of the combination of high angles of attack (21.2°) and sideslip (20°) which were experienced immediately prior to compressor surge.

Four of the surges for airplane B that are neither in nor near the surge boundary occurred at Mach numbers greater than 1.35. Reference 4 indicates that above this Mach number a surge problem existed until the lower portion of the leading edge of the boundary-layer splitter plate was cambered toward the fuselage, which prevented flow separation on the plate and reduced boundary-layer buildup. The airplane of this paper did not have the cambered splitter plate.

If separation occurred on the plate for these surges, it would be expected that circumferential distortion would occur at the compressor face. By comparing the values of the root-mean-square distortions for surge conditions (table I) with nonsurge conditions (fig. 16), it is seen that no significant difference existed between root-mean-square distortion for surge and root-mean-square distortion for nonsurge. However, the root-mean-square distortion is a distortion index which gives a mean value of the overall distortion, without distinction between radial distortion and circumferential distortion. Therefore, it is possible that, if for a particular case the circumferential distortion is "high," the root-mean-square value may mask this if the radial distortion is "low." As seen in table I, the circumferential distortion index D (taken from ref. 5) gives higher circumferential distortion values for every surge that occurred for Mach numbers greater than 1.35 than for the surges at lower Mach numbers and at total pressures less than about 500 pounds per square foot.

For the other point outside the wind-tunnel surge region for airplane B the circumferential distortion is higher than for the points in, or near, the surge region. This high distortion is believed to be the result of high angle of attack (10.6°) of the airplane prior to surge.

CONCLUDING REMARKS

Measurements of total-pressure recovery and distortion at the compressor face for the test airplanes having similar two-spool turbojet engines, but with dissimilar inlets, indicate that: The total-pressure recovery was relatively independent of angle of attack and mass-flow ratio for both airplanes, except for a significant decrease in pressure recovery with angle of attack for airplane B at the highest Mach numbers tested. The root-mean-square total-pressure distortion decreased slightly with angle of attack and increased slightly with mass-flow ratio for

airplane A. For airplane B the distortion increased with angle of attack and decreased slightly with mass-flow ratio, particularly at the higher altitudes. Altitude effects on distortion were noted only for airplane B.

Several compressor surges were encountered for each airplane primarily in the region of high altitude and low inlet total pressure, as was indicated by wind-tunnel tests. At lower altitudes and at higher inlet total pressures, surges were encountered under conditions of high total-pressure distortion, particularly circumferential distortion.

High-Speed Flight Station,
National Advisory Committee for Aeronautics,
Edwards, Calif., February 25, 1958.

REFERENCES

1. Saltzman, Edwin J.: Flight-Determined Induction-System and Surge Characteristics of the YF-102 Airplane With a Two-Spool Turbojet Engine. NACA RM H57C22, 1957.

2. Matranga, Gene J., and Peele, James R.: Flight-Determined Static Lateral Stability and Control Characteristics of a Swept-Wing Fighter Airplane to a Mach Number of 1.39. NACA RM H57A16, 1957.

3. Capasso, Vincent N., Jr., and Schalk, Louis W.: F-101 Phase IV Stability and Control Test. AFFTC TR 56-14, Air Research and Development Command, U.S. Air Force, July 1956.

4. Pavlick, J. F., and Valor, N. H.: Model F-101A - A Summary of the Engine Stall Problem and Its Elimination. Contract No. AF33(600)-8743, Rep. No. 4545, McDonnell Aircraft Corp., Jan. 5, 1956.

5. Alford, J. S.: Inlet Flow Distortion Index. GER-1404, General Electric Co. Presented at the International Days of Aeronautical Sciences, Paris, France, May 27 to 29, 1957.

[redacted]

TABLE I

FLIGHT AND COMPRESSOR-FACE CONDITIONS PRIOR TO SURGE

Airplane	M_0	h_p, ft	α, deg	p_0, lb/sq ft	p'_0, lb/sq ft	M_c	$R \times 10^{-6}$	p'_c, lb/sq ft	T', $^\circ R$	N, rpm	$\frac{N}{\sqrt{\theta_c}}$, rpm	w_a, lb/sec	$\frac{w_a\sqrt{\theta_c}}{\delta_c}$, lb/sec	m/m_0	p'_c/p'_0	S, percent	D, percent	$\sqrt{\theta_c}$	δ_c
A	0.756	39,470	21.2	401	586	0.370	3.58	543	477	8,220	8,930	46.5	164	0.729	0.925	8.1	6.5	0.9208	0.2609
	.810	48,480	7.5	261	402	.565	2.63	392	436	9,220	10,050	40.4	200	.810	.976	5.5	2.0	.9175	.1854
	.695	48,010	9.4	260	360	.508	2.15	352	427	9,030	9,950	33.8	184	.808	.979	3.9	2.0	.9074	.1665
B	1.374	38,950	8.4	412	1,209	0.440	6.29	1,101	541	9,870	9,670	85.6	159	0.913	0.911	5.2	8.5	1.021	0.5486
	1.438	30,780	6.1	457	2,165	.373	9.00	1,776	577	9,790	9,200	115.1	146	.832	.874	4.3	8.4	1.065	.8393
	1.035	42,070	10.6	387	1,700	.482	4.05	651	476	9,890	10,130	58.6	186	.956	.930	5.7	8.8	.9765	.3076
	1.477	38,350	4.0	424	1,507	.409	6.96	1,293	556	10,000	9,500	93.8	161	.894	.858	4.5	7.2	1.052	.6111
	1.478	38,010	4.5	431	1,535	.409	6.96	1,302	564	9,880	9,500	94.7	160	.893	.848	5.0	9.3	1.040	.6153
	1.120	50,880	9.3	242	508	.490	2.70	477	491	9,950	10,200	42.4	183	.985	.938	6.1	6.7	.9756	.2254
	1.037	51,710	4.0	224	443	.485	2.47	415	477	9,750	10,200	37.6	183	.970	.937	6.3	5.2	.9560	.1961
	1.056	50,800	9.0	234	468	.497	2.70	437	480	9,880	10,300	40.6	189	.984	.934	6.5	5.9	.9596	.2065
	1.034	52,090	4.8	220	428	.493	2.47	404	476	9,860	10,280	37.4	188	.987	.944	6.7	5.7	.9596	.1909
	1.042	51,710	9.8	224	443	.496	2.47	414	478	9,750	10,200	37.9	185	.977	.930	7.5	6.8	.9551	.1956
	.945	50,350	7.5	239	425	.444	2.47	385	456	9,700	10,350	31.9	164	.924	.907	7.4	6.0	.9372	.1819
C	0.598	43,300	12.4	335	426	0.454	1.52	381	424	8,700	9,670	31.8	160	0.935	0.892	3.7	1.6	0.9035	0.1800
	.588	43,300	11.0	335	423	.414	1.52	398	423	8,400	9,300	30.8	148	.901	.915	3.3	1.6	.9032	.1881
	.587	43,300	10.8	335	423	.415	1.52	387	423	8,380	9,280	31.0	153	.906	.915	3.2	1.8	.9030	.1830
	.594	42,700	12.5	344	437	.509	1.52	382	427	8,810	9,730	34.3	172	.991	.874	4.2	3.0	.9054	.1805
	.757	48,300	9.2	264	386	.561	1.60	333	435	9,000	10,000	30.7	176	.898	.863	4.7	4.8	.9000	.1574
	.778	50,100	8.9	242	361	.572	1.37	312	405	9,180	10,150	28.6	176	.898	.863	4.7	4.2	.9049	.1474
	.756	49,250	9.4	252	368	.556	1.37	321	404	8,880	9,850	29.1	173	.875	.865	4.1	4.0	.9015	.1517
	.808	49,900	8.5	244	375	.556	1.44	327	432	9,150	10,080	29.6	174	.882	.873	4.0	5.5	.9082	.1545
	.630	44,200	10.4	320	418	.583	1.52	350	413	9,320	10,550	35.0	187	.854	.872	4.0	---	.8841	.1654

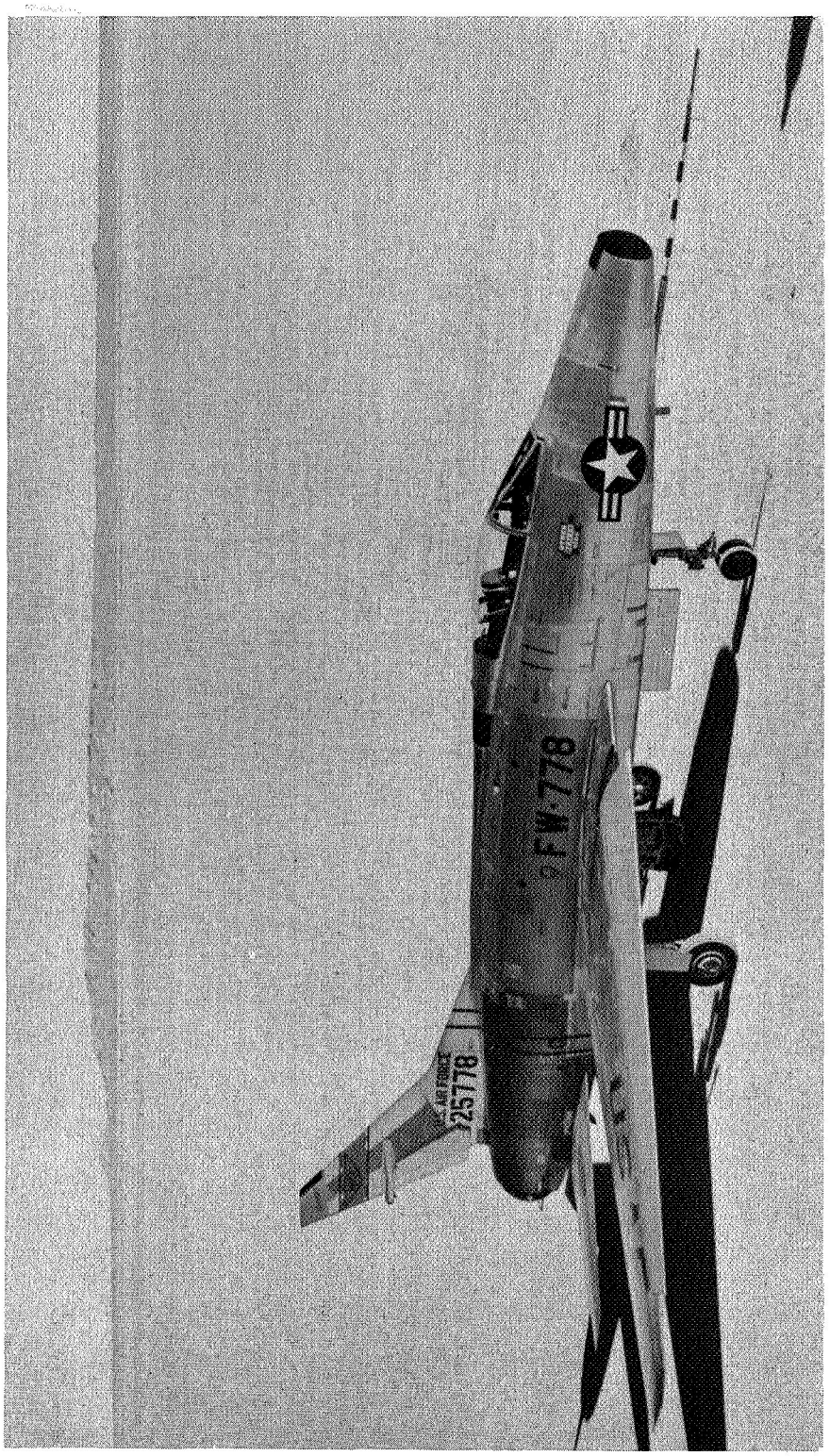

Figure 1.- Photograph of airplane A. E-2097

[redacted]

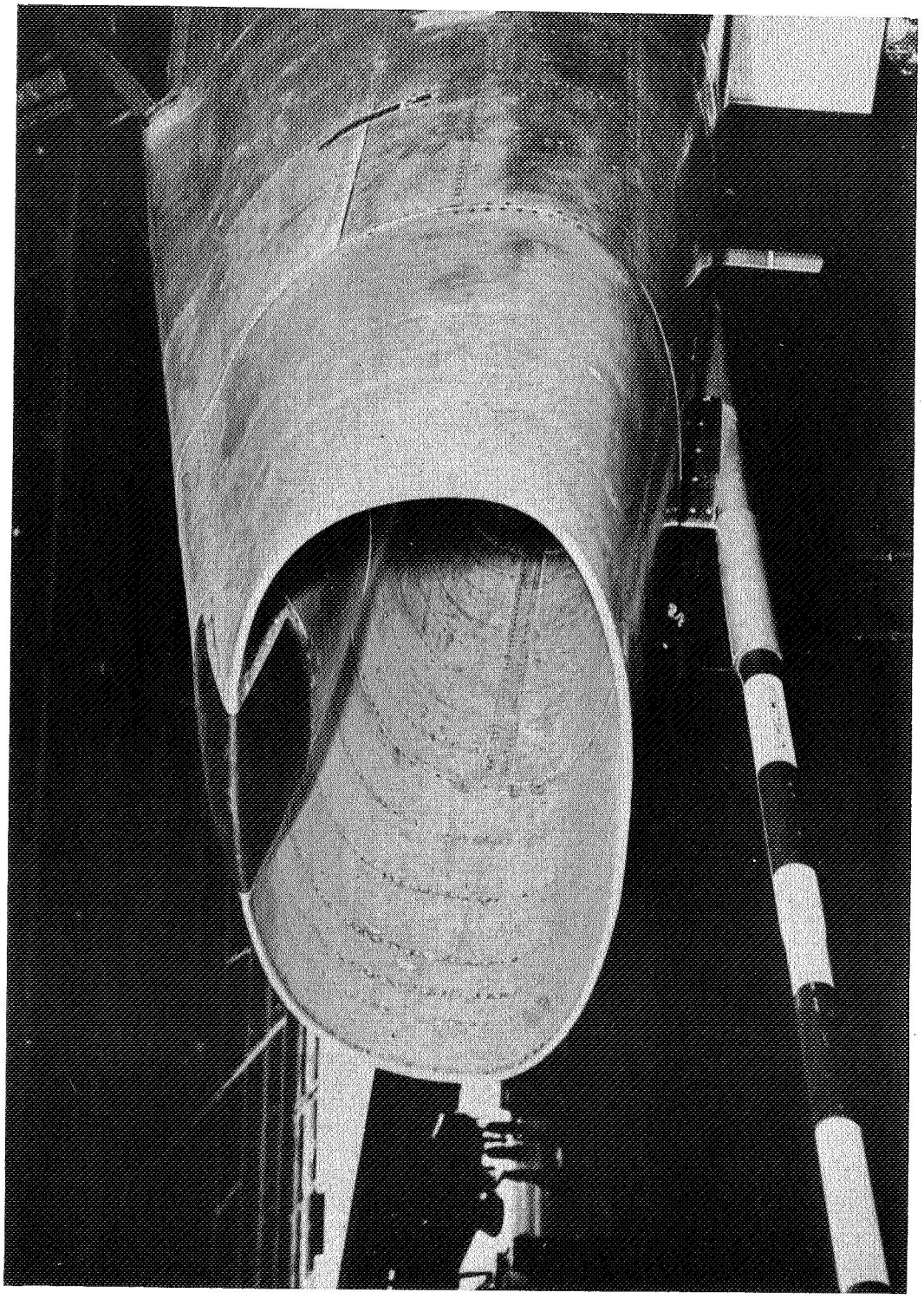

Figure 2.- Photograph showing inlet of airplane A. E-2994

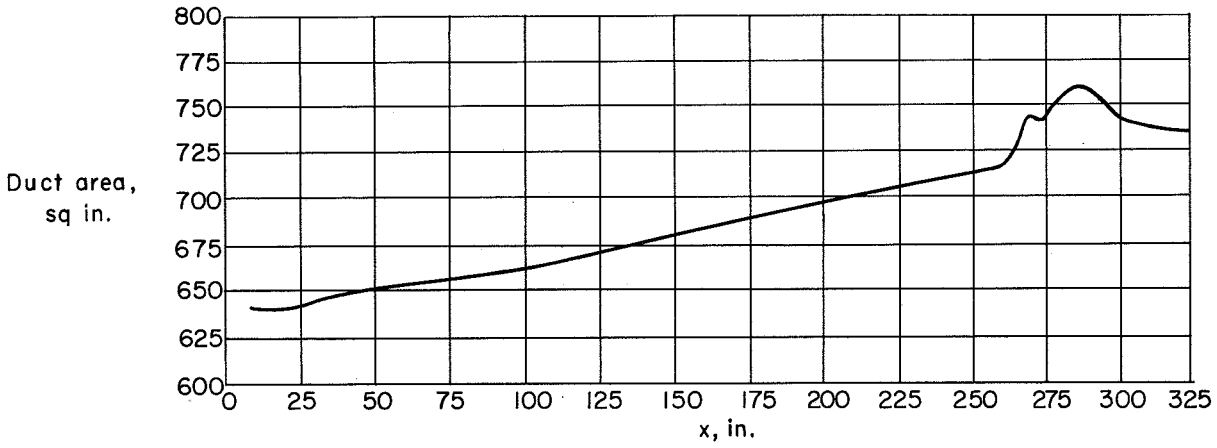

(a) Longitudinal variation of duct cross-sectional area.

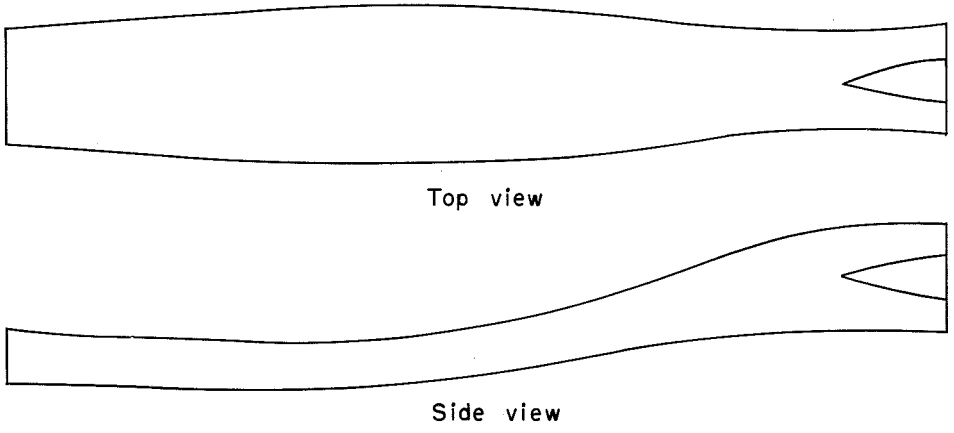

(b) Geometric duct characteristics.

Figure 3.- Geometric duct characteristics and longitudinal variation of duct cross-sectional area for airplane A.

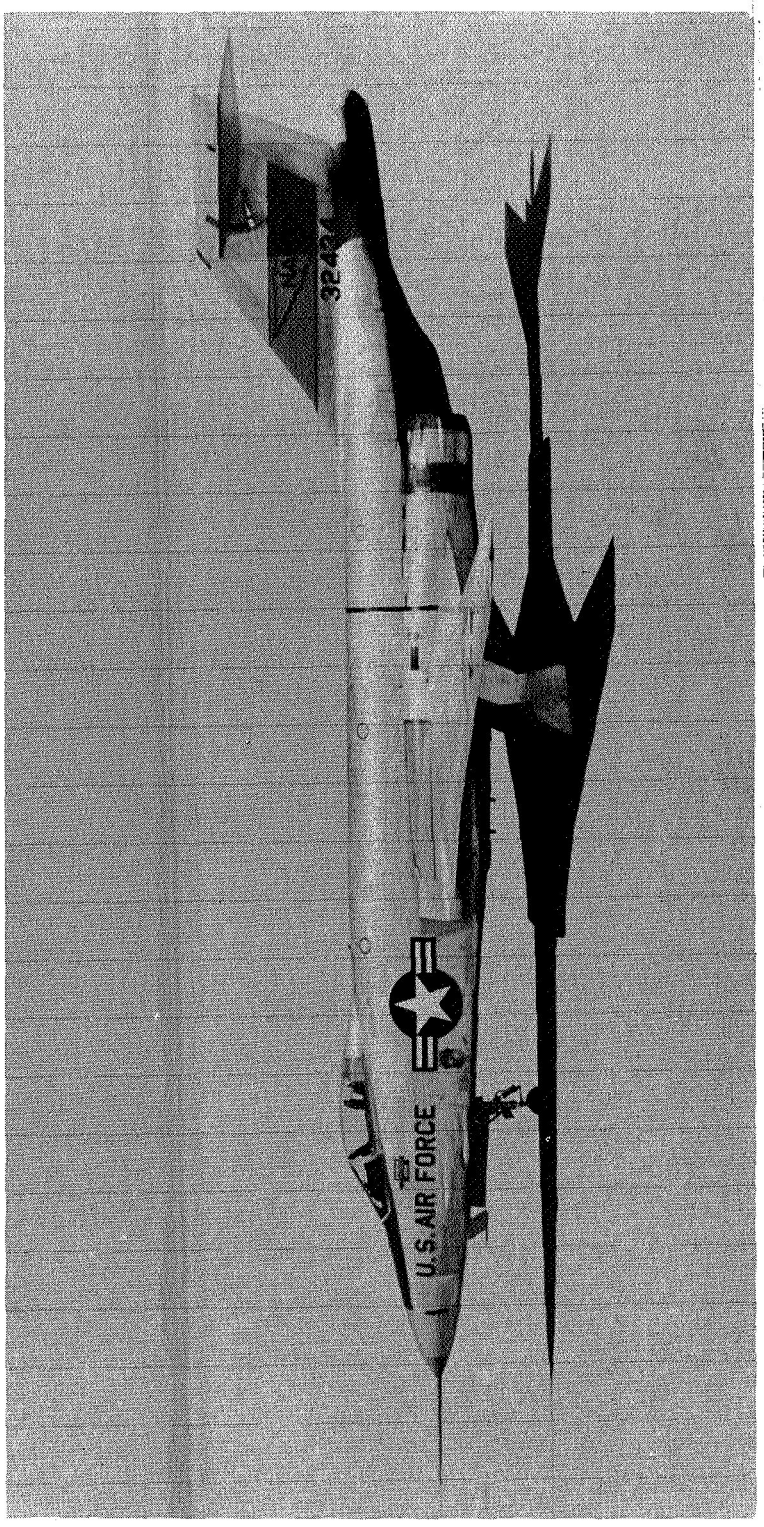

Figure 4.- Photograph of airplane B. E-2455

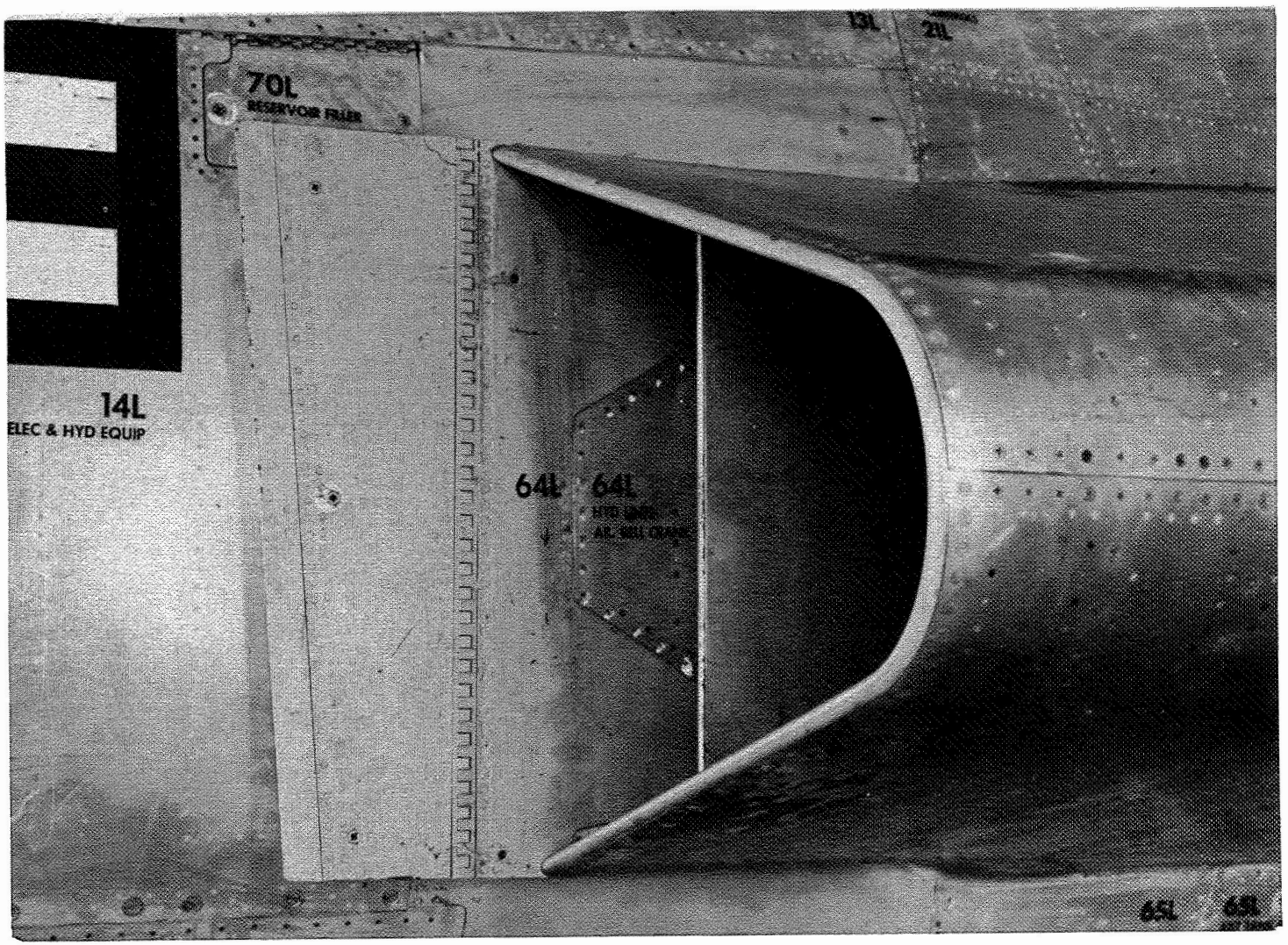

Figure 5.- Photograph showing left inlet of airplane B. E-2459

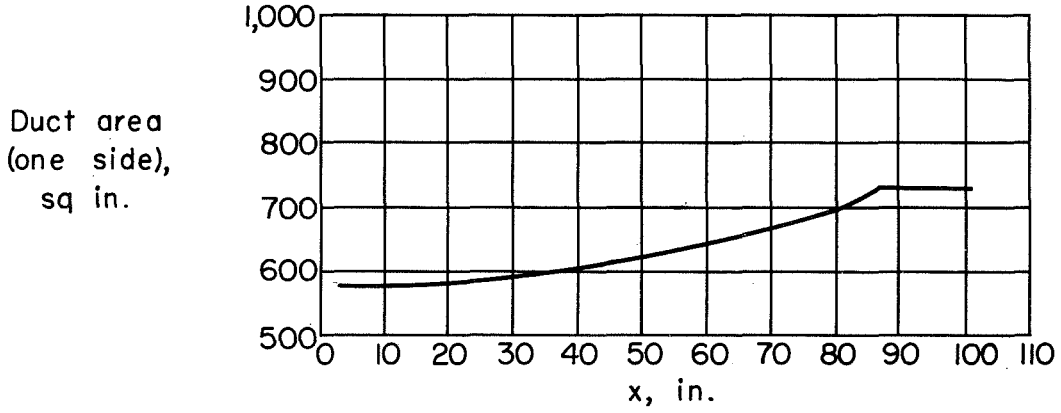

(a) Longitudinal variation of duct cross-sectional area.

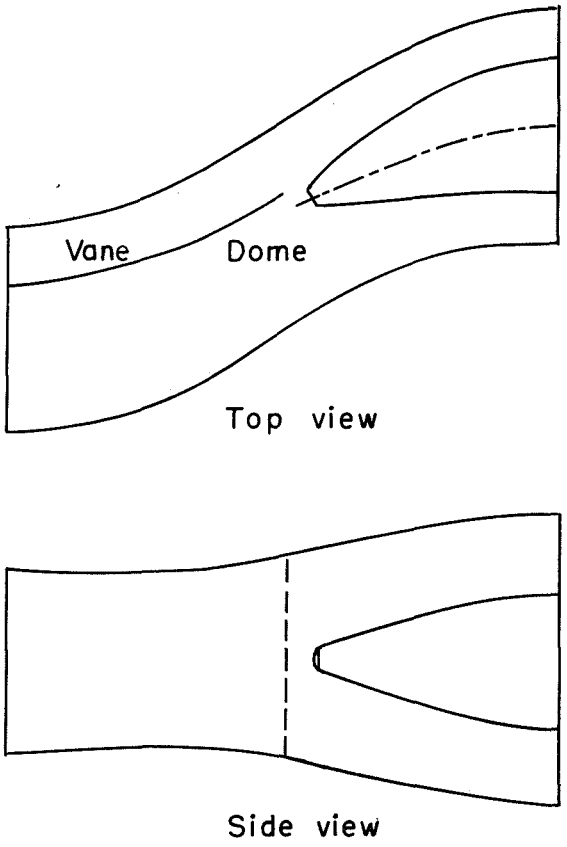

(b) Geometric duct characteristics.

Figure 6.- Geometric duct characteristics and longitudinal variation of duct cross-sectional area for airplane B.

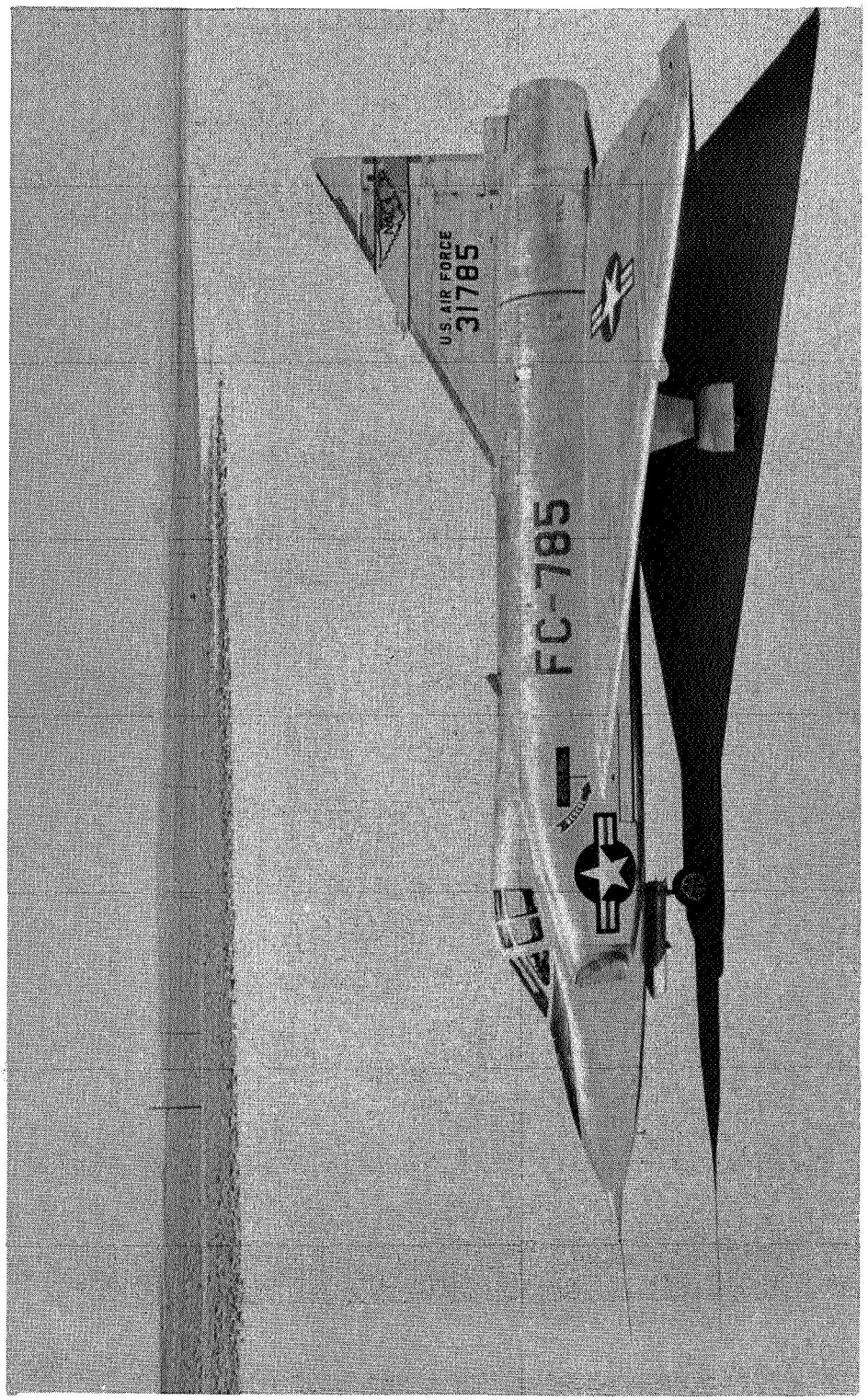

Figure 7.- Photograph of airplane C. E-1747

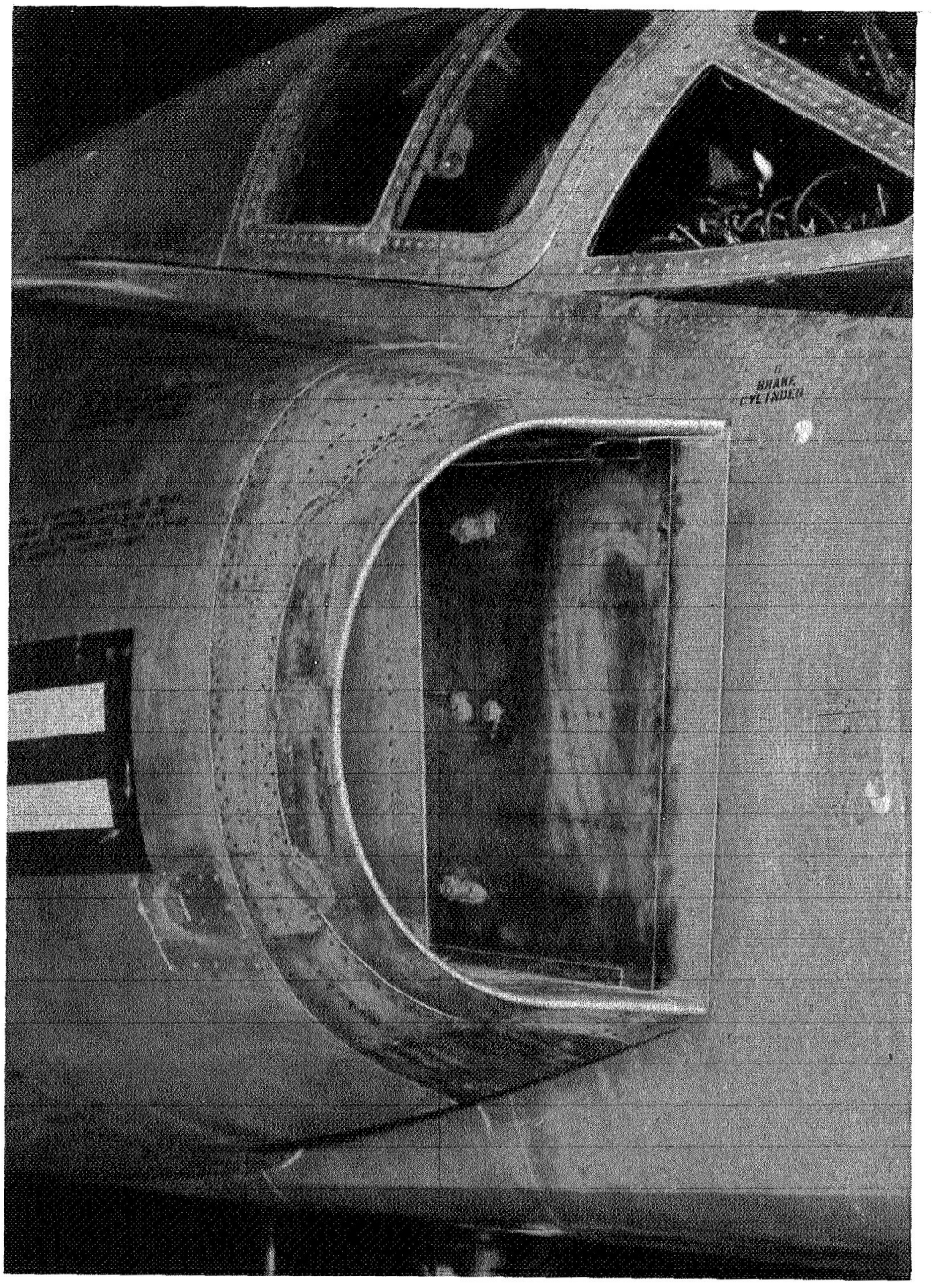

Figure 8.- Photograph showing right inlet of airplane C. E-2760

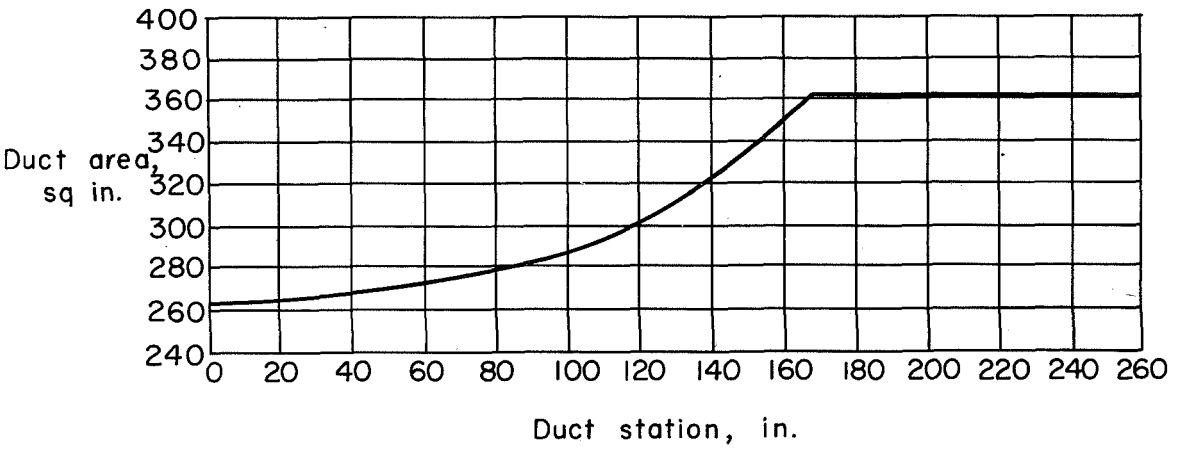

(a) Longitudinal variation of duct cross-sectional area.

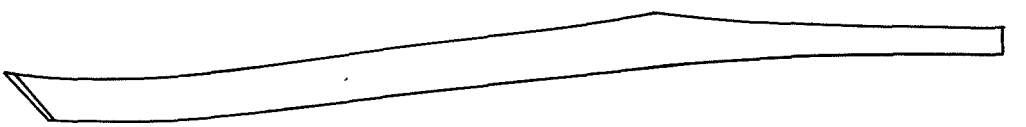

Top view

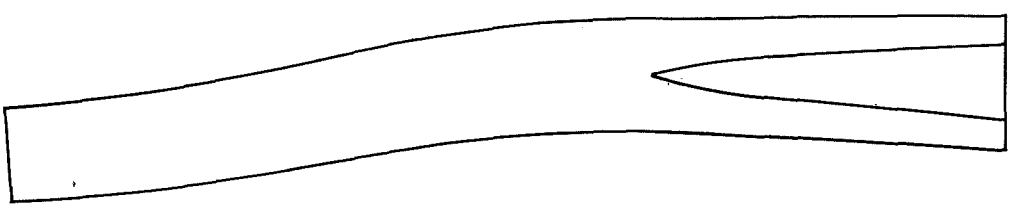

Side view

(b) Geometric duct characteristics.

Figure 9.- Geometric duct characteristics and longitudinal variation of duct cross-sectional area for airplane C.

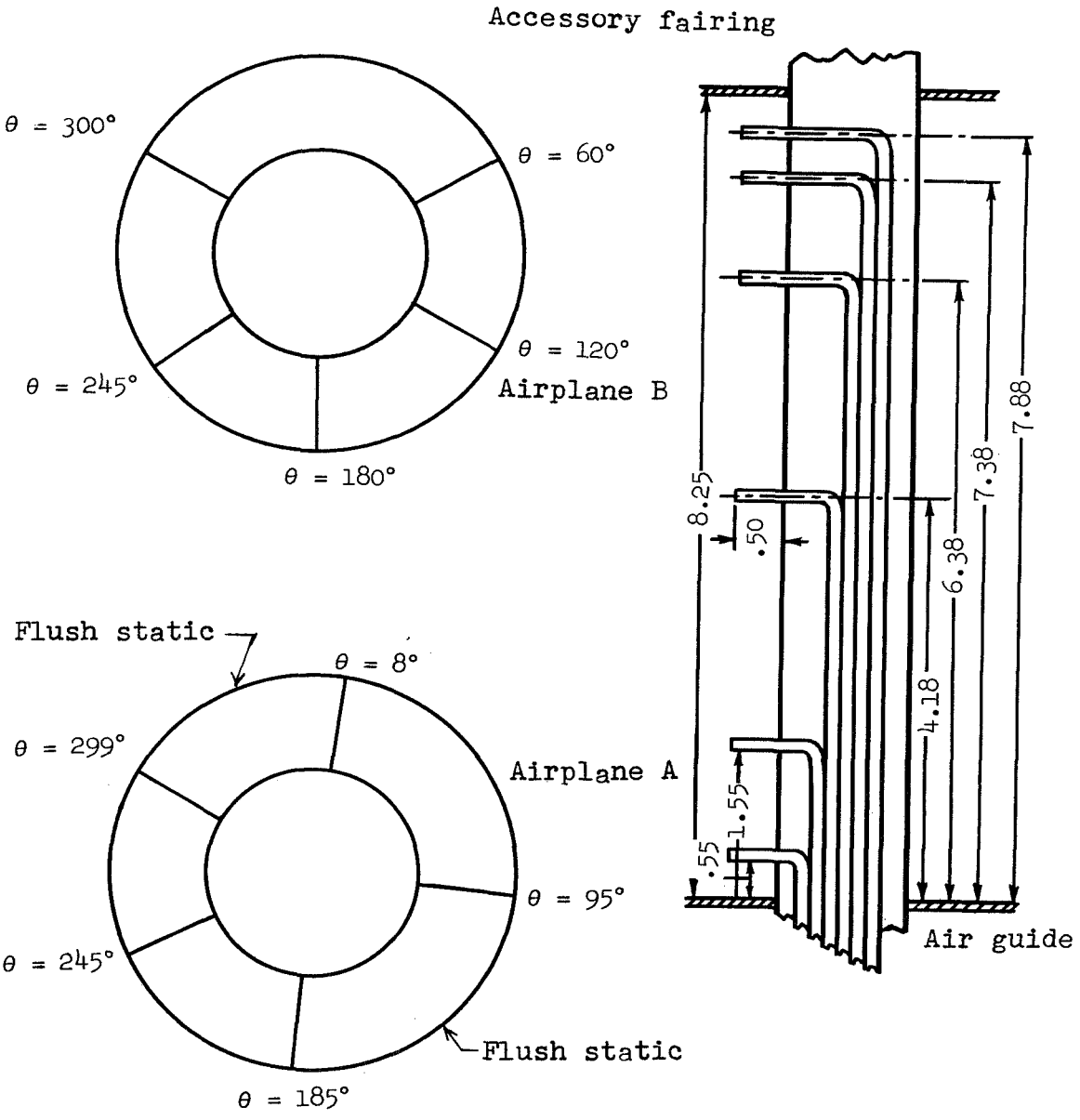

(a) Rake arrangement of compressor face looking aft.

(b) Details of rakes.

Figure 10.- Compressor-face instrumentation for airplanes A and B.

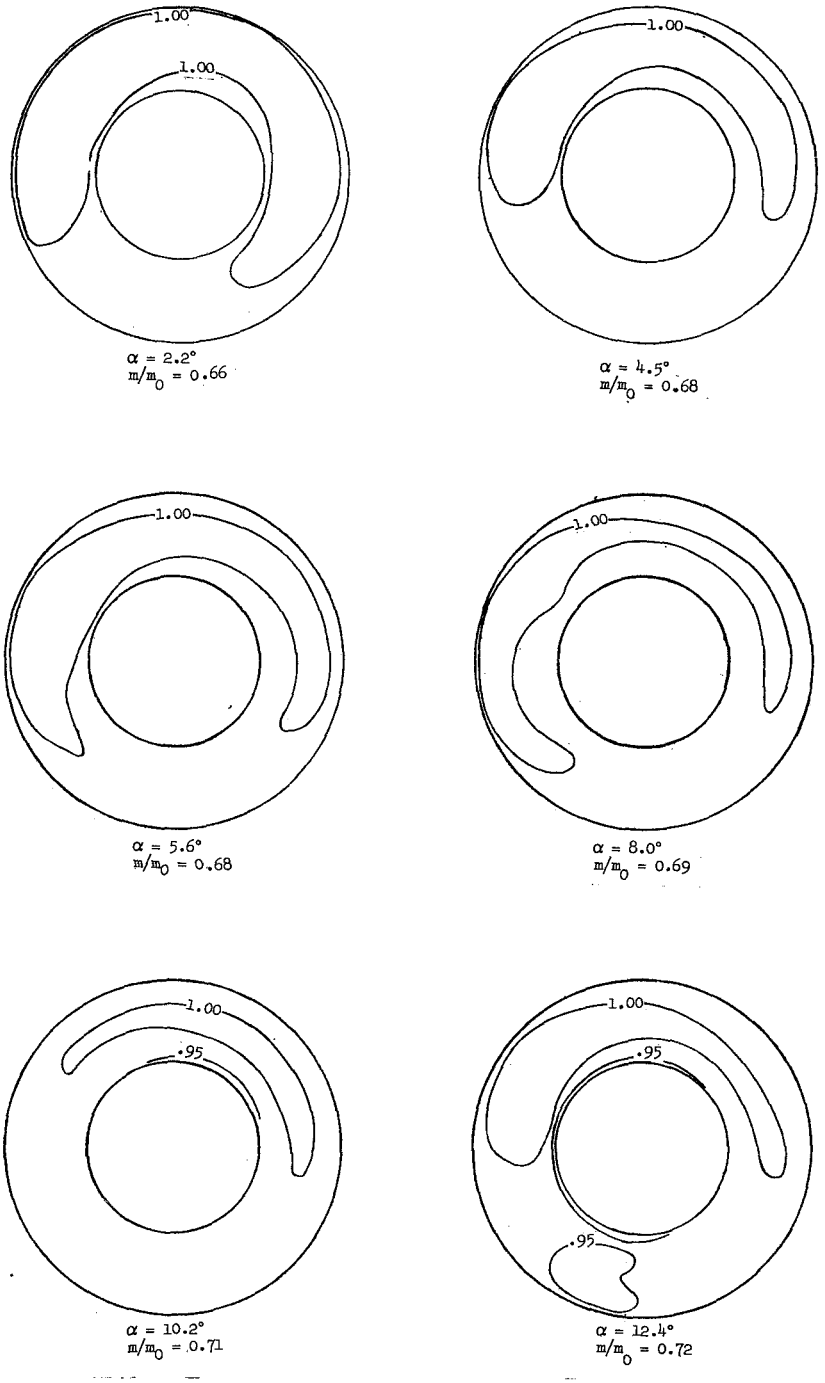

(a) $M \approx 0.80$; $h_p \approx 22{,}000$ feet.

Figure 11.- Total-pressure-recovery contours at the compressor face with angle of attack for airplane A.

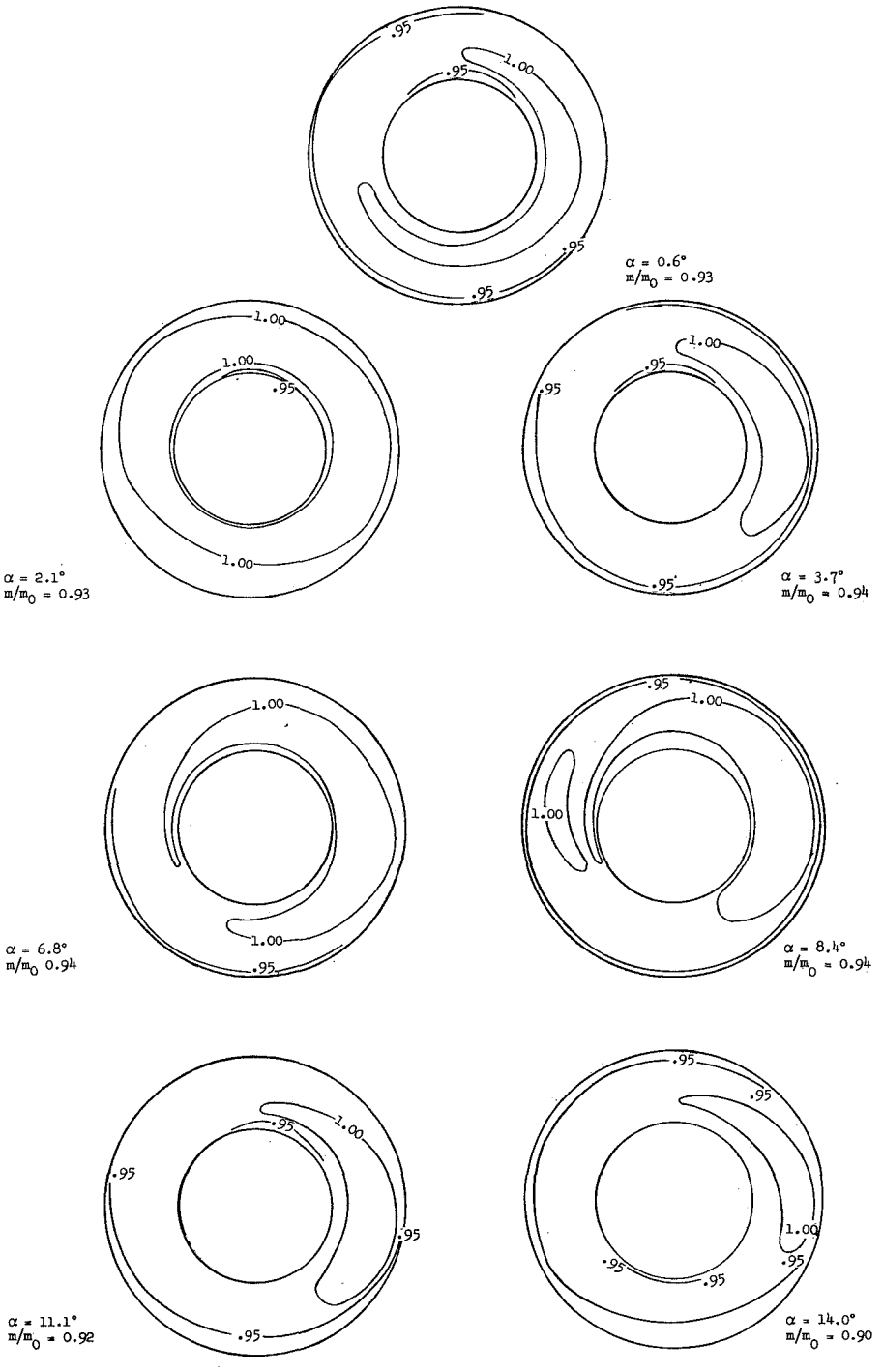

(b) $M \approx 1.0$; $h_p \approx 40{,}000$ feet.

Figure 11.- Continued.

[redacted]

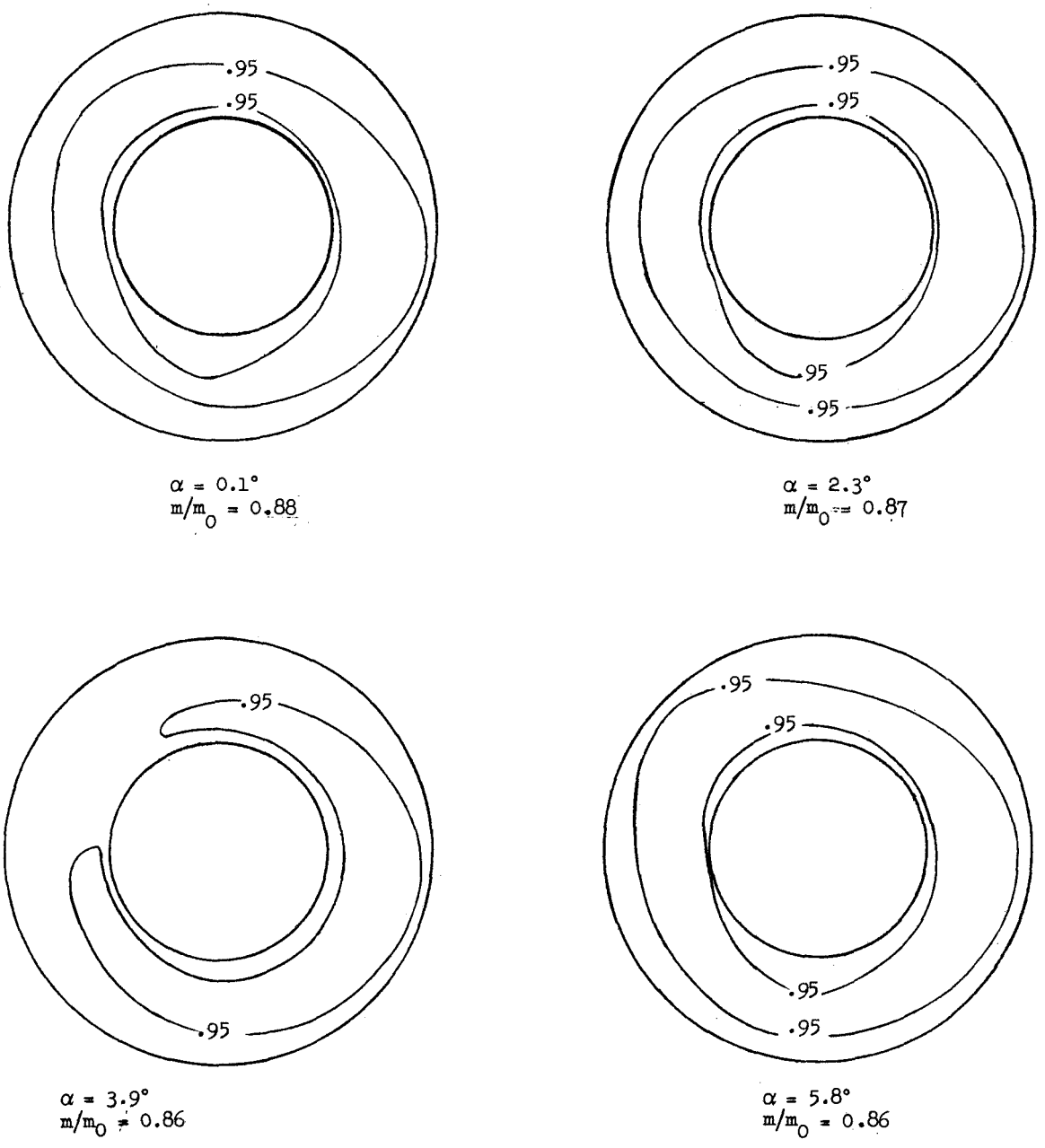

(c) $M \approx 1.4$; $h_p \approx 33{,}500$ feet.

Figure 11.- Concluded.

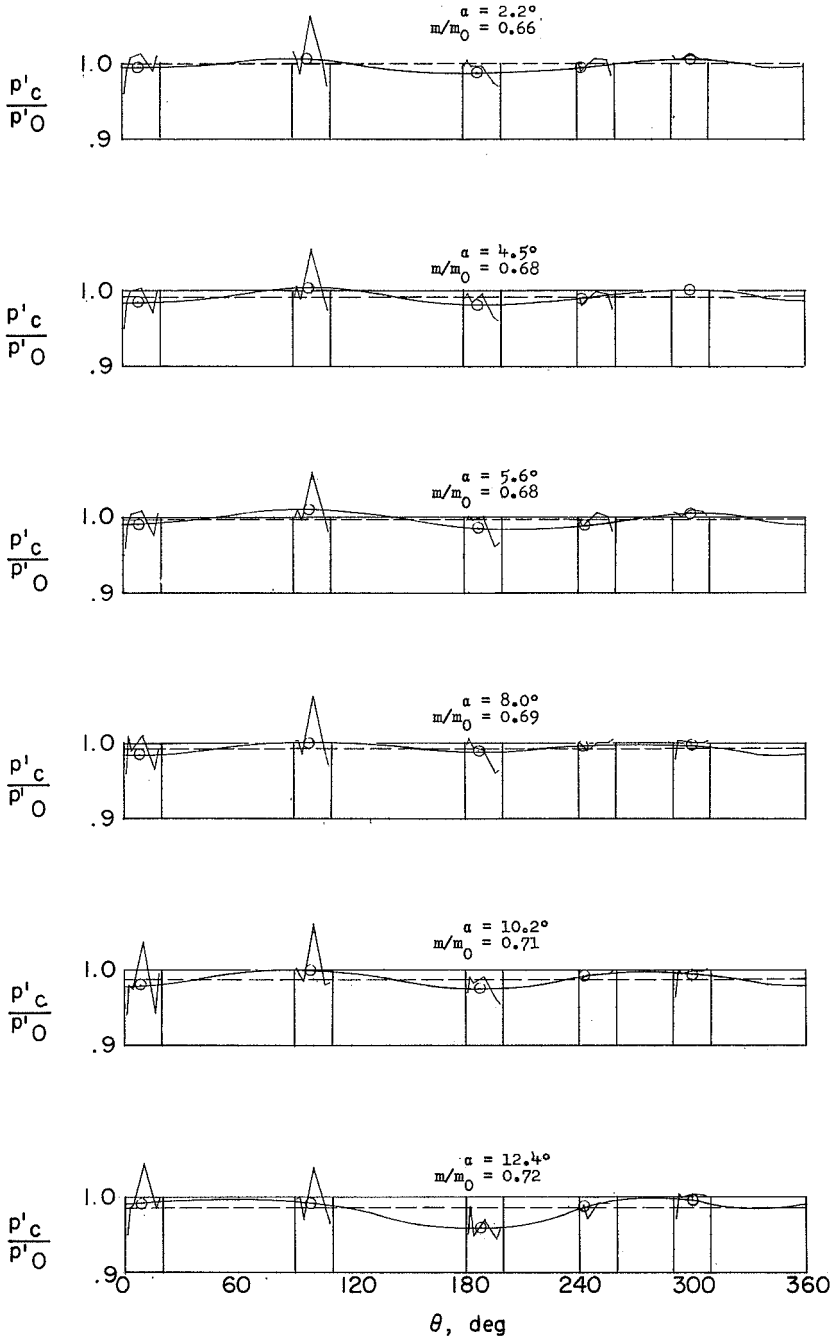

(a) $M \approx 0.80$; $h_p \approx 22{,}000$ feet.

Figure 12.- Circumferential and radial total-pressure-recovery profiles for different angles of attack for airplane A.

[redacted]

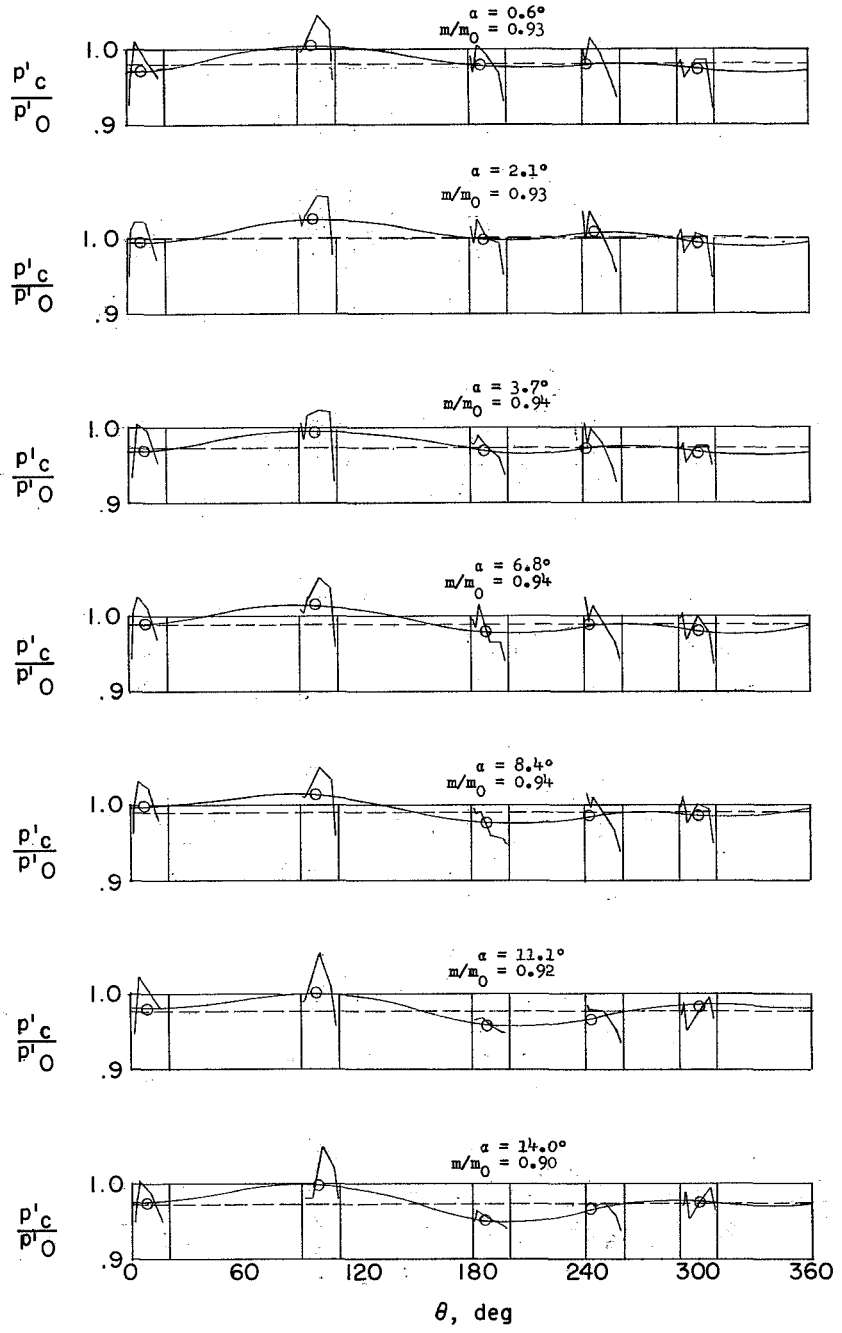

(b) $M \approx 1.0$; $h_p \approx 40{,}000$ feet.

Figure 12.- Continued.

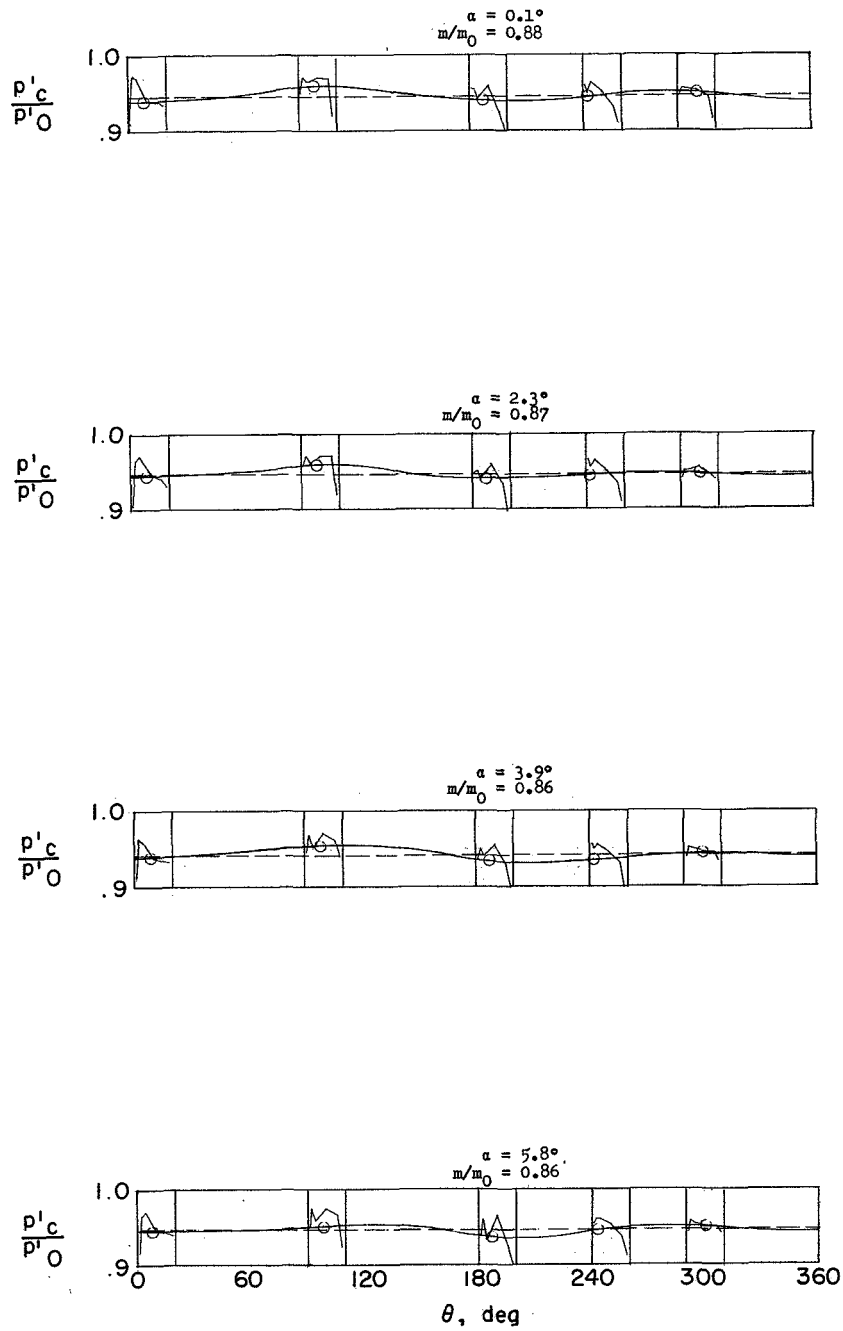

(c) $M \approx 1.40$; $h_p \approx 33{,}500$ feet.

Figure 12.- Concluded.

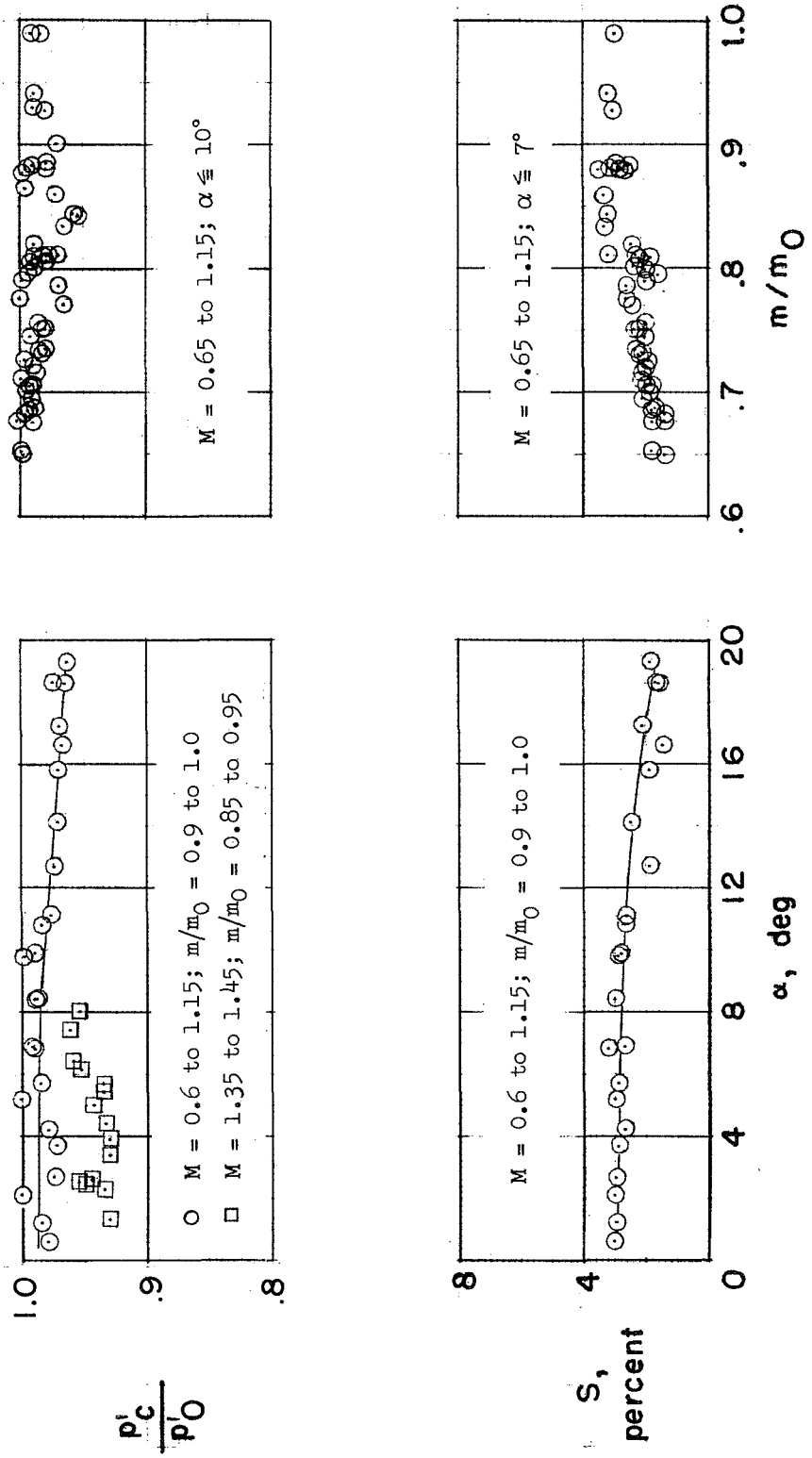

Figure 13.- Average total-pressure recovery and root-mean-square total-pressure distortion with angle of attack and mass-flow ratio for airplane A.

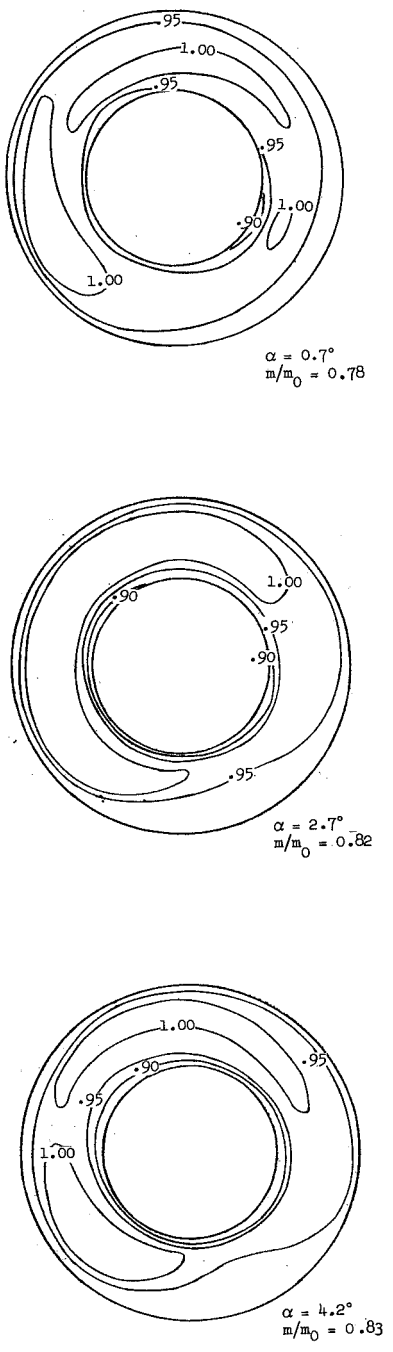

(a) $M \approx 0.9$; $h_p \approx 26{,}500$ feet.

Figure 14.- Total-pressure-recovery contours at the compressor face with angle of attack for airplane B.

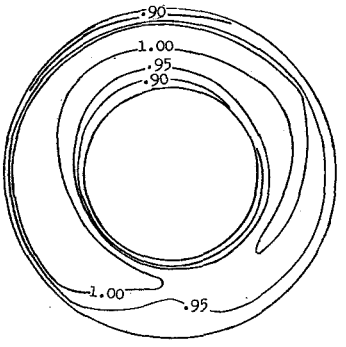

$\alpha = 3.3°$
$m/m_0 = 1.00$

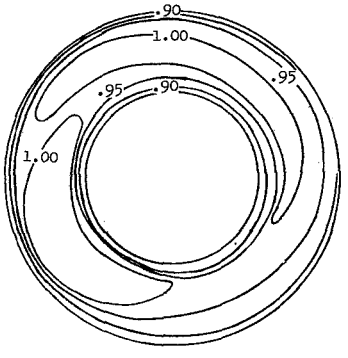

$\alpha = 5.1°$
$m/m_0 = 0.98$

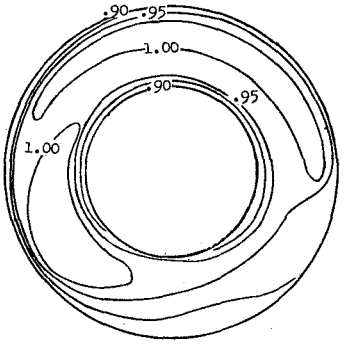

$\alpha = 7.4°$
$m/m_0 = 0.98$

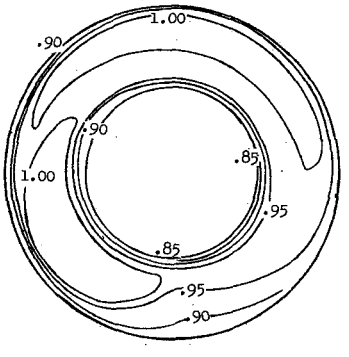

$\alpha = 8.5°$
$m/m_0 = 0.99$

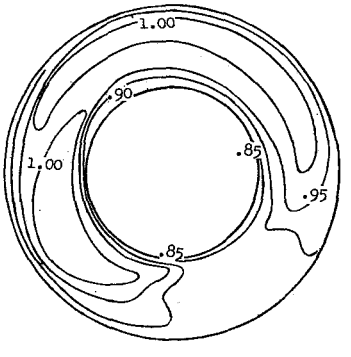

$\alpha = 10.7°$
$m/m_0 = 0.96$

(b) $M \approx 1.05$; $h_p \approx 42{,}000$ feet.

Figure 14.- Continued.

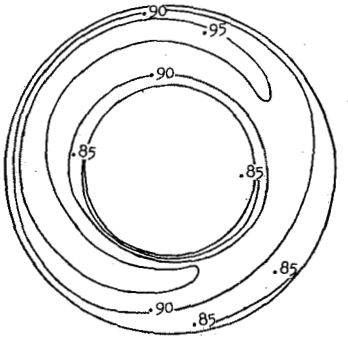

$\alpha = 2.0°$
$m/m_0 = 0.87$

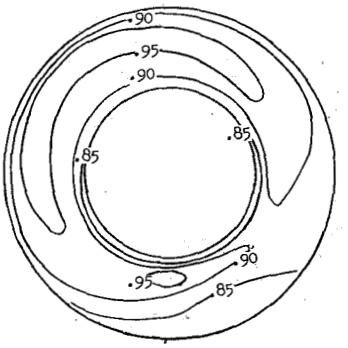

$\alpha = 3.8°$
$m/m_0 = 0.85$

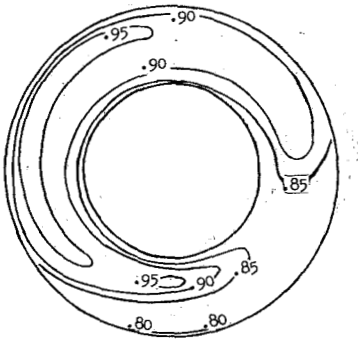

$\alpha = 6.1°$
$m/m_0 = 0.82$

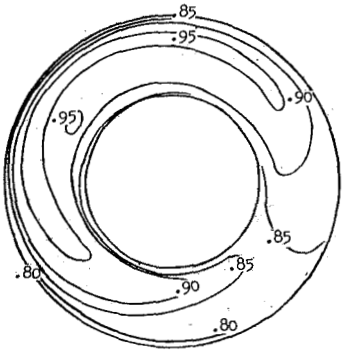

$\alpha = 7.9°$
$m/m_0 = 0.82$

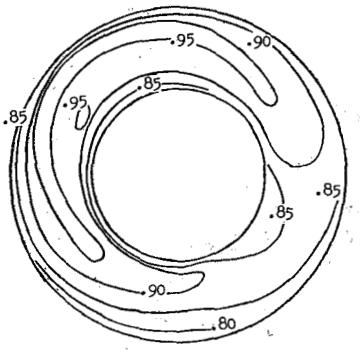

$\alpha = 8.5°$
$m/m_0 = 0.82$

(c) $M \approx 1.40$; $h_p \approx 39{,}000$ feet to $41{,}000$ feet.

Figure 14.- Concluded.

[redacted]

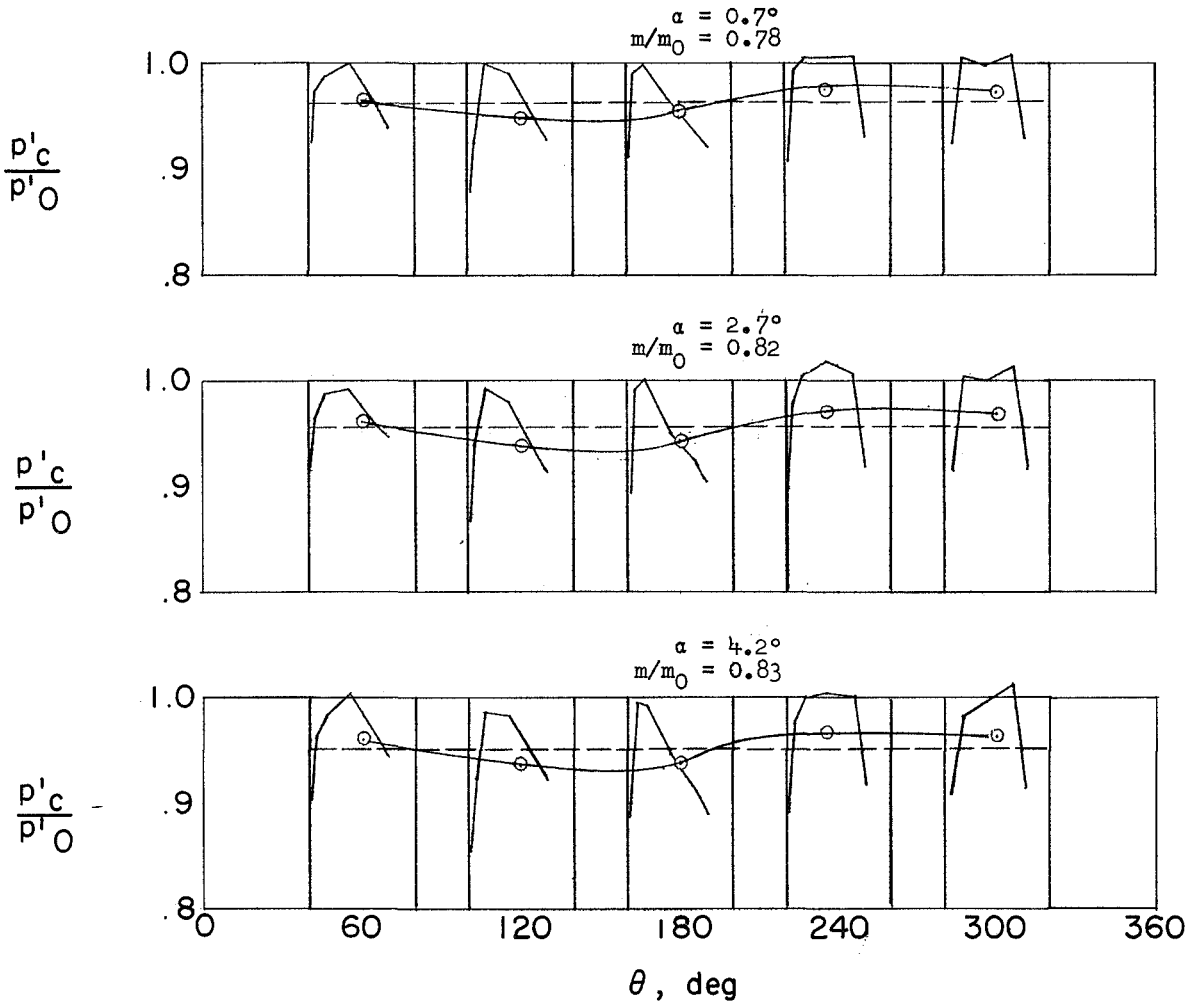

(a) $M \approx 0.9$; $h_p \approx 26{,}500$ feet.

Figure 15.- Circumferential and radial total-pressure-recovery profiles for different angles of attack for airplane B.

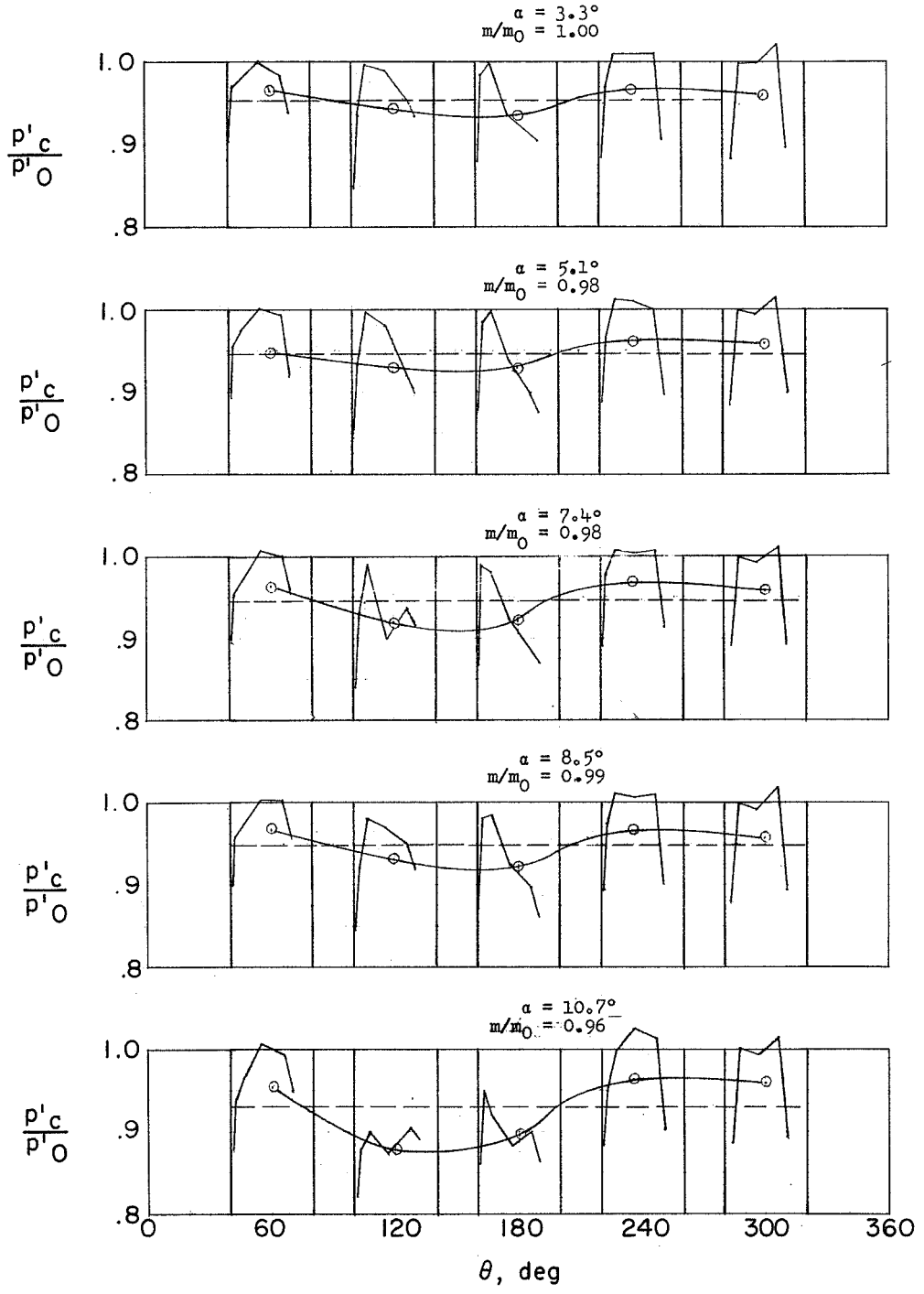

(b) $M \approx 1.05$; $h_p \approx 42{,}000$ feet.

Figure 15.- Continued.

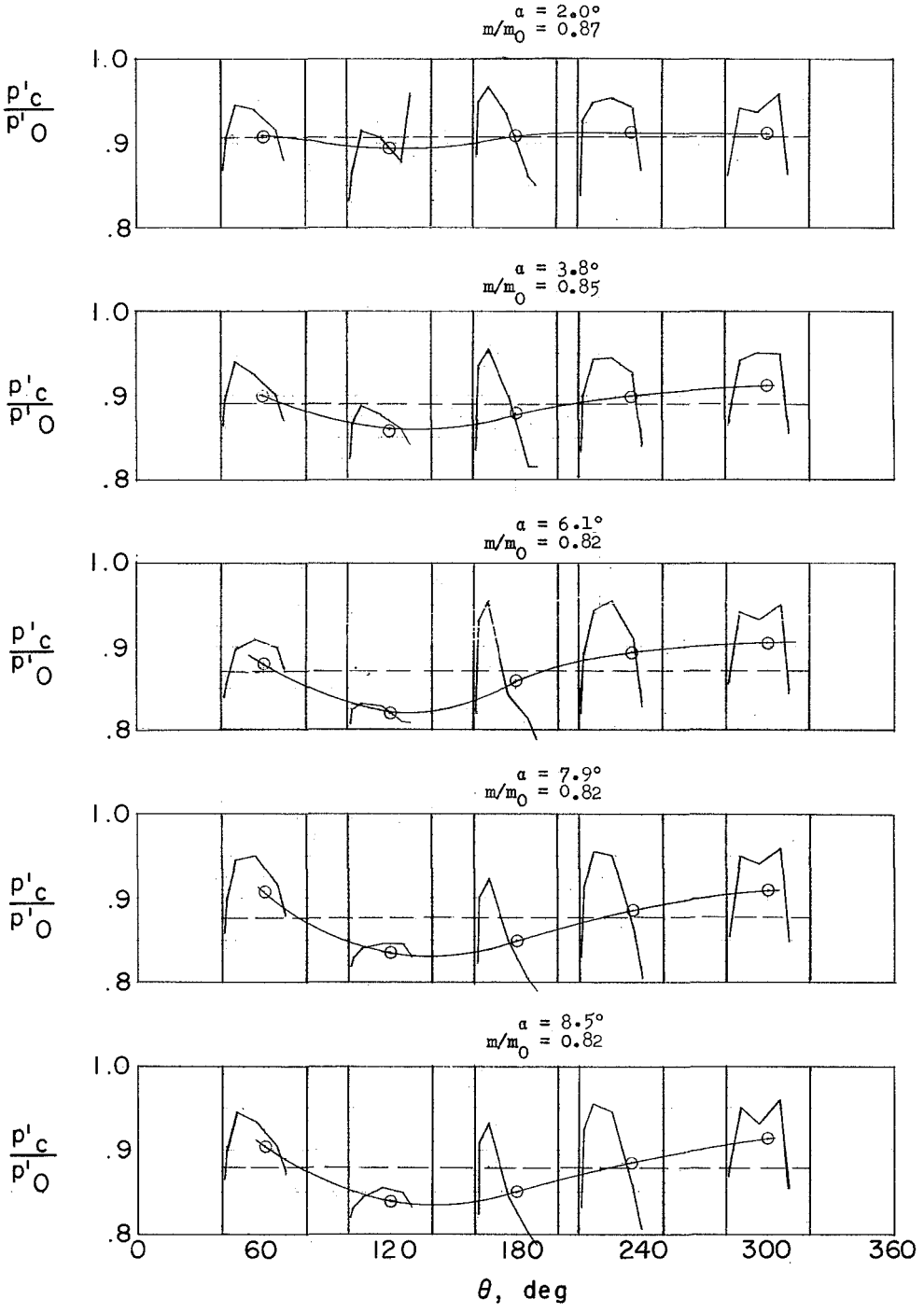

(c) $M \approx 1.40$; $h_p \approx 39{,}000$ feet to 41,000 feet.

Figure 15.- Concluded.

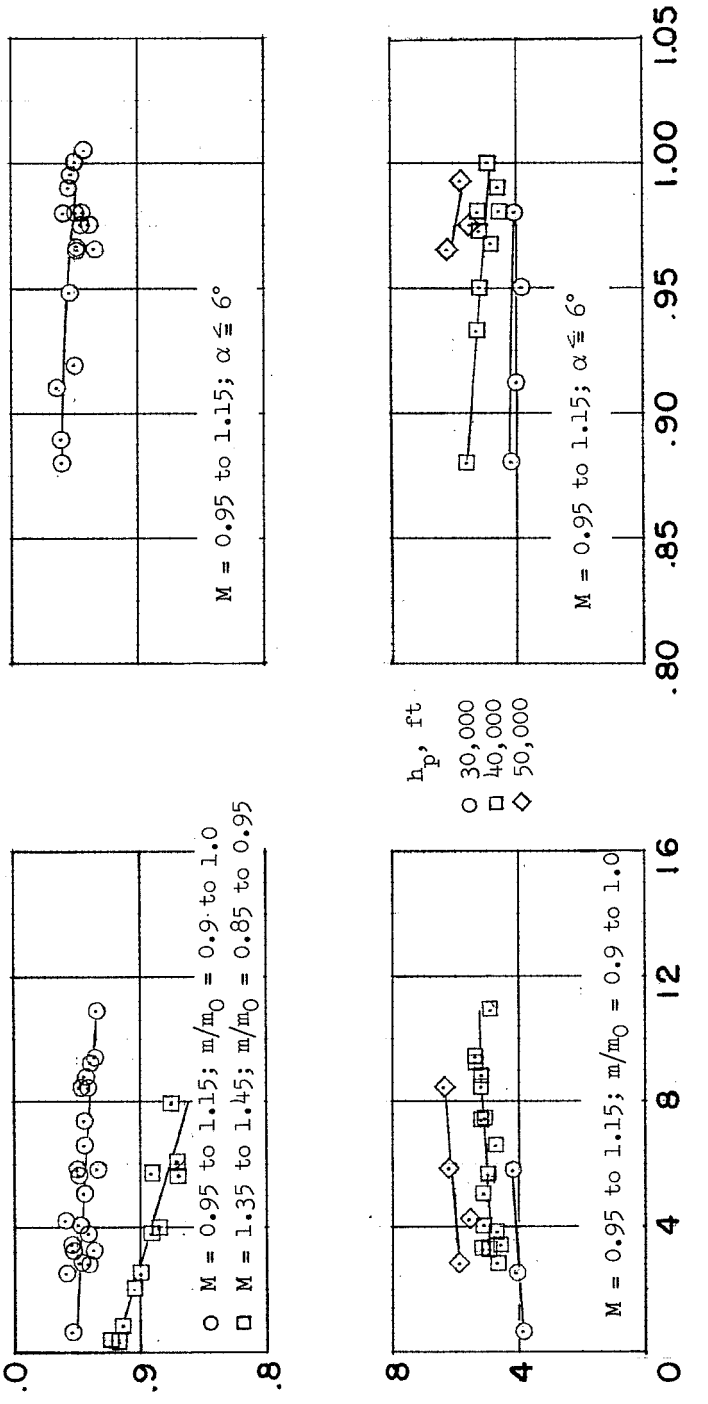

Figure 16.- Average total-pressure recovery and root-mean-square total-pressure distortion with angle of attack and mass-flow ratio for airplane B.

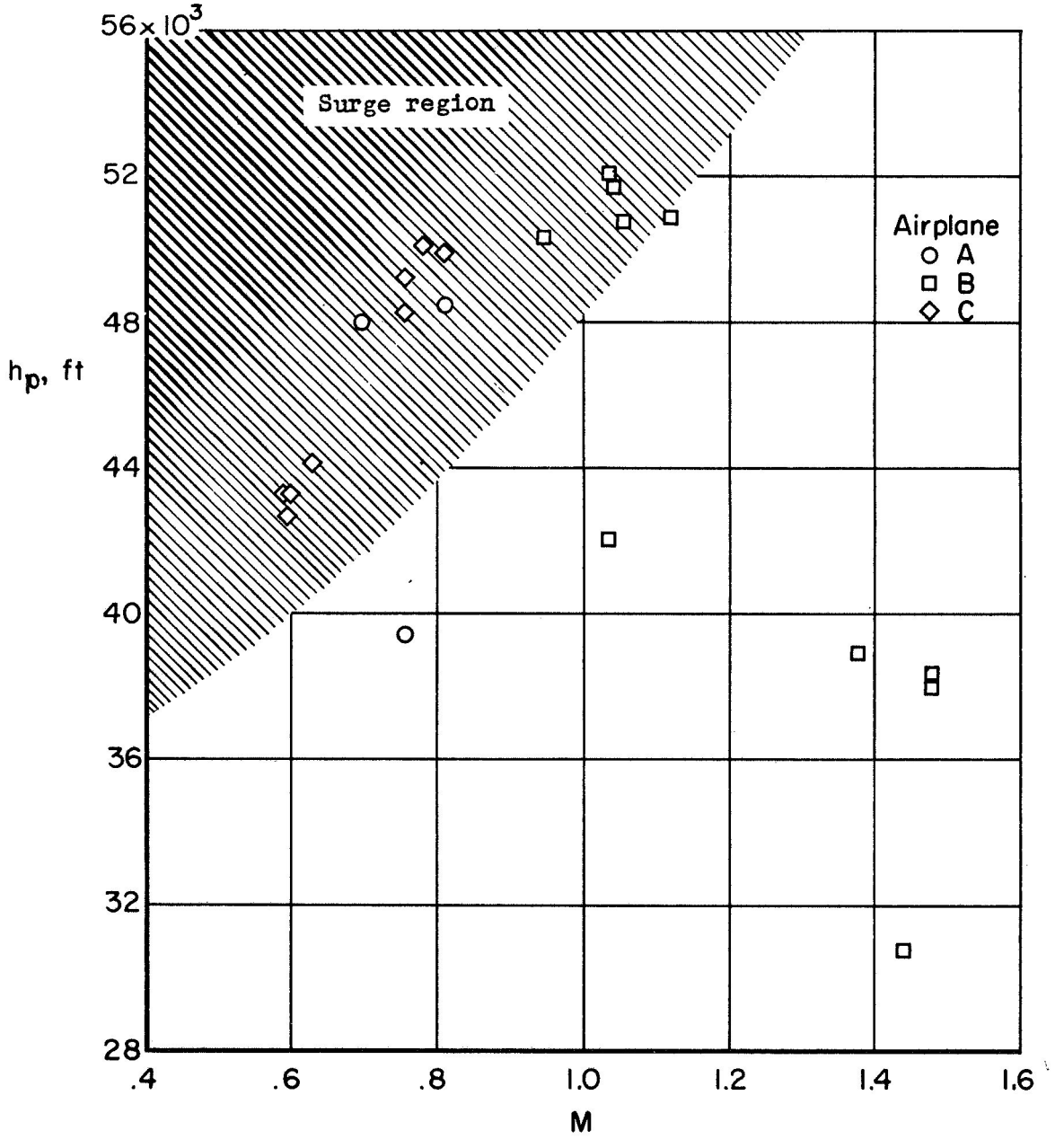

Figure 17.- Pressure altitude and Mach number at incidence of surge for airplanes A, B, and C.

NOTES: (1) Reynolds number is based on the diameter of a circle with the same area as that of the capture area of the inlet.

(2) The symbol * denotes the occurrence of buzz.

Report and facility	Description			Test parameters				Test data				Performance		Remarks
	Configuration	Number of oblique shocks	Type of boundary-layer control	Free-stream Mach number	Reynolds number $\times 10^{-6}$	Angle of attack, deg	Angle of yaw, deg	Drag	Inlet-flow profile	Discharge-flow profile	Flow picture	Maximum total-pressure recovery	Mass-flow ratio	
CONFID. RM H58C14 NACA High-Speed Flight Station		None	None	0.6 to 1.45	2.6 to 8.8	0 to 21	±20			X		99%	0.63 to 0.99	Compressor surge data included
CONFID. RM H58C14 NACA High-Speed Flight Station		None	None	0.6 to 1.45	2.6 to 8.8	0 to 21	±20			X		99%	0.63 to 0.99	Compressor surge data included
CONFID. RM H58C14 NACA High-Speed Flight Station		None	None	0.6 to 1.45	2.6 to 8.8	0 to 21	±20			X		99%	0.63 to 0.99	Compressor surge data included
CONFID. RM H58C14 NACA High-Speed Flight Station		None	None	0.6 to 1.45	2.6 to 8.8	0 to 21	±20			X		99%	0.63 to 0.99	Compressor surge data included

Bibliography

These strips are provided for the convenience of the reader and can be removed from this report to compile a bibliography of NACA inlet reports. This page is being added only to inlet reports and is on a trial basis.

NOTES: (1) Reynolds number is based on the diameter of a circle with the same area as that of the capture area of the inlet.

(2) The symbol * denotes the occurrence of buzz.

Report and facility	Description			Test parameters				Test data				Performance		Remarks
	Configuration	Number of oblique shocks	Type of boundary-layer control	Free-stream Mach number	Reynolds number $\times 10^{-6}$	Angle of attack, deg	Angle of yaw, deg	Drag	Inlet-flow profile	Discharge-flow profile	Flow picture	Maximum total-pressure recovery	Mass-flow ratio	
CONFID. RM H58C14 NACA High-Speed Flight Station		One	Splitter	0.9 to 1.5	2.5 to 9.2	0 to 11	±2			X		96%	0.79 to 1.00	Compressur surge data included
CONFID. RM H58C14 NACA High-Speed Flight Station	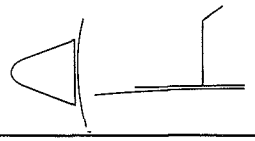	One	Splitter	0.9 to 1.5	2.5 to 9.2	0 to 11	±2			X		96%	0.79 to 1.00	Compressor surge data included
CONFID. RM H58C14 NACA High-Speed Flight Station	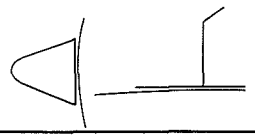	One	Splitter	0.9 to 1.5	2.5 to 9.2	0 to 11	±2			X		96%	0.79 to 1.00	Compressor surge data included
CONFID. RM H58C14 NACA High-Speed Flight Station	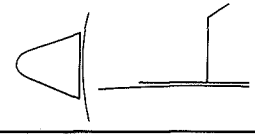	One	Splitter	0.9 to 1.5	2.5 to 9.2	0 to 11	±2			X		96%	0.79 to 1.00	Compressor surge data included

Bibliography

These strips are provided for the convenience of the reader and can be removed from this report to compile a bibliography of NACA inlet reports. This page is being added only to inlet reports and is on a trial basis.

NOTES: (1) Reynolds number is based on the diameter of a circle with the same area as that of the capture area of the inlet.

(2) The symbol * denotes the occurrence of buzz.

Report and facility	Description			Test parameters				Test data				Performance		Remarks
	Configuration	Number of oblique shocks	Type of boundary-layer control	Free-stream Mach number	Reynolds number $\times 10^{-6}$	Angle of attack, deg	Angle of yaw, deg	Drag	Inlet-flow profile	Discharge-flow profile	Flow picture	Maximum total-pressure recovery	Mass-flow ratio	
CONFID. RM H58C14 NACA High-Speed Flight Station		One	Splitter	0.6 to 0.8	1.4 to 1.6	0 to 12	±3							Data presented only for conditions immediately prior to surge
CONFID. RM H58C14 NACA High-Speed Flight Station		One	Splitter	0.6 to 0.8	1.4 to 1.6	0 to 12	±3							Data presented only for conditions immediately prior to surge
CONFID. RM H58C14 NACA High-Speed Flight Station		One	Splitter	0.6 to 0.8	1.4 to 1.6	0 to 12	±3							Data presented only for conditions immediately prior to surge
CONFID. RM H58C14 NACA High-Speed Flight Station		One	Splitter	0.6 to 0.8	1.4 to 1.6	0 to 12	±3							Data presented only for conditions immediately prior to surge

Bibliography

These strips are provided for the convenience of the reader and can be removed from this report to compile a bibliography of NACA inlet reports. This page is being added only to inlet reports and is on a trial basis.